Investigation of Gas Migration in saturated Argillaceous Rock

DISSERTATION

zur Erlangung des akademischen Grades

Doctor-Ingenieur

(Dr.-Ing.)

vorgelegt

der Fakultät Umweltwissenschaften
der Technischen Universität Dresden

von

M.Sc. Wenjie Xu
geboren am 09.08.1984 in Zhejiang, China

Gutachter:
Herr Prof. Dr.-Ing. habil. Olaf Kolditz
Helmholtz-Zentrum für Umweltforschung UFZ und Technische Universität Dresden

Herr Prof. Dr.-Ing. habil. Michael Zhengmeng Hou
Technische Universität Clausthal

Herr Prof. Ph.D. Weimin Ye
Tongji Universität, Shanghai, China

Verteidigung am: 22.11.2013

Erklärung des Promovenden

Die Übereinstimmung dieses Exemplars mit dem Original der Dissertation zum Thema:

„Investigation of Gas Migration in saturated Argillaceous Rock"

wird hiermit bestätigt.

Hannover, 08.04.2013
Ort, Datum

………………………………….……
Unterschrift   (Wenjie Xu)

Zusammenfassung

In dieser Arbeit wird die Gasmigration in gesättigtem Tonstein untersucht. Abhängig von der Höhe des Gasdrucks wird der Gastransportprozess von unterschiedlichen Mechanismen kontrolliert. Gasinjektionsversuchen sind durchgeführt worden, um den Gastransportprozess in gering permeablem Tonstein zu untersuchen. Der Fokus der Arbeit liegt auf Opalinuston, der Gegenstand zahlreicher Studien war und eine große Bedeutung bei der Suche nach möglichen Wirtsgesteinen für die Endlagerung radioaktiver Abfälle spielt. Gasinjektiontsversuchen in unterschiedlichen Maßstäben (Laborversuchen, In-situ-Bohrloch- und In-situ-Tunnelversuchen) werden intensiv untersucht. Die Versuchsergebnisse werden analysiert und mit numerischen Modellierungsverfahren interpretiert.

Ein numerisches Modell für die Kopplung zwischen Mehrphasenströmung und Mechanik ist entwickelt und im wissenschaftlichen Berechnungsprogramm OpenGeoSys (OGS) implementiert worden. In diesem Model wird die Beziehung zwischen Kapillardruck und Wassersättigungsgrad mit der Funktion nach van Genuchten beschrieben. Das Darcy Gesetz wird für den Strömungsprozess mit Berücksichtigung der relativen Permeabilität der Wasser- und Gasphase angewandt. Der Verformungsprozess wird anhand von einem elasto-perfekt-plastischen Modell berechnet. Das anisotrope hydraulische und mechanische Verhalten von Opalinuston wird im numerischen Modell berücksichtigt. Die hydraulische Anisotropie wird vom Permeabilitätstensor kontrolliert. Der elastische Verformungsprozess wird mit dem verallgemeinerten hookeschen Gesetz berechnet. Der „return mapping"-Algorithmus wird für das plastische Verhalten verwendet. Die Anisotropie der Plastizität wird mit einem sogenannten „microstructrue tensor" Verfahren berücksichtigt. Die Permeabilitätsänderung bei der Gasinjektion wird durch eine druckabhängige oder verformungsabhängige Formulierung beschrieben. Durch die Berücksichtigung der Permeabilitätsentwicklung können die Versuchsergebnisse im numerischen Modell quantitative repräsentiert und die beobachteten Phänomene interpretiert werden.

Unter Laborbedingungen kann festgestellt werden, dass die Permeabilität eines Probekörpers bei Kompression reduziert wird. Eine erhebliche Permeabilitätserhörung findet statt, wenn der Gasdruck höher als der Manteldruck ist. Unter In-situ-Bedingungen können geschädigte Zonen durch die Auffahrung von Bohrlöchern oder Tunneln generiert werden. Der stark durchlässige Bereich in der geschädigten Zone dominiert den Strömungsprozess. Fluid kann durch die geschädigte Zone in den nicht abgedichteten Bereich fließen, wie z. B. in das seismische Beobachtungsbohrloch beim In-situ-Bohrlochversuchen oder in den Bereich außerhalb des Megapackers beim In-situ-Tunnelversuchen.

In dieser Arbeit werden die von Zweiphasenströmung und von Fließwegdilatanz kontrollierten Gasmigrationsmechanismen erfolgreich simuliert. Das entwickelte numerische Modell kann für die Untersuchung von Gasinjektionsversuchen bei unterschiedlichen Maßstäben verwendet werden.

Abstract

Gas migration in saturated argillaceous rock is studied in this work. Dependent on the pressure level the gas transport process is controlled by different mechanisms. Gas injection tests have been carried to investigate the gas transport process in low permeable argillaceous rock. We focus on the Opalinus Clay, which has been widely researched and is important for searching possible host rock of the radioactive waste disposal. Gas injection tests at different scales (laboratory, in-situ borehole and in-situ tunnel test) are intensively investigated in this work. The measurements of the tests are analysed and interpreted with numerical modelling method.

A coupled multi-phase flow and mechanical model has been developed and implemented in the scientific computed codes OpenGeoSys (OGS). In the applied numerical model the relationship between capillary pressure and water saturation degree is described with van Genuchten model. The Darcy's law is used for the phase flux, and the relative permeability of both water and gas phase is considered. The deformation process is calculated with elastic perfect-plastic model. The anisotropic hydraulic and mechanic behaviours of the Opalinus Clay are involved in the numerical model. The hydraulic anisotropy is controlled by the permeability tensor. The elastic deformation process is modelled by generalized Hooke's law. The plastic behaviour is calculated with return mapping algorithm, and the anisotropy is considered with a so called microstructure tensor method. The permeability change during the gas injection is described using pressure dependent or deformation dependent approach. With considering the permeability evolution the measured data can be in the numerical model quantitatively represented, and test observations can be interpreted.

Under laboratory condition it can be determined that the specimen permeability is reduced during compression. The significant permeability increase takes places when the gas injection pressure higher than the confining pressure. By the in-situ tests damage zone can be generated due to the drilling of boreholes and tunnel. The highly permeable areas dominate the hydraulic process. Fluid flows through the damaged zone into the not sealed section, e.g. the seismic observation boreholes by the in-situ borehole tests and the section out of the megapacker by the in-situ tunnel tests.

In this work, the two phase flow controlled and pathway dilatancy controlled gas migration mechanisms are successfully simulated. The developed numerical model can be used to investigate the gas injection tests at different scales and conditions.

Acknowledgments

Contents

1. INTRODUCTION

1.1 Motivation and objectives

Gas migration in an engineered barrier system and in the host rock is an important issue for management of final disposal of radioactive waste in deep geological underground. In the post closure phase of a nuclear waste disposal system gases can be produced as a result of corrosion of metal canister, degradation of organic matter and radiolysis of water (NAGRA 2004). Due to gas generation the pressure in a repository will be increased. Under high gas pressure the mechanical and hydraulic properties of the host rock and barrier system can be significantly changed, which may lead to the release of gases. Therefore, hydro-mechanical analysis is required to evaluate the long-term safety of a disposal system.

Fig. 1 shows possible gas flow pathways out of a L/ILW repository: 1) along the excavation induced damage zone, 2) through insufficient sealing material, and 3) into the host rock through pore space. To this end, the investigation and study of gas transport in the repository system is one of the most important issues for the long-term safety analysis of a final disposal project.
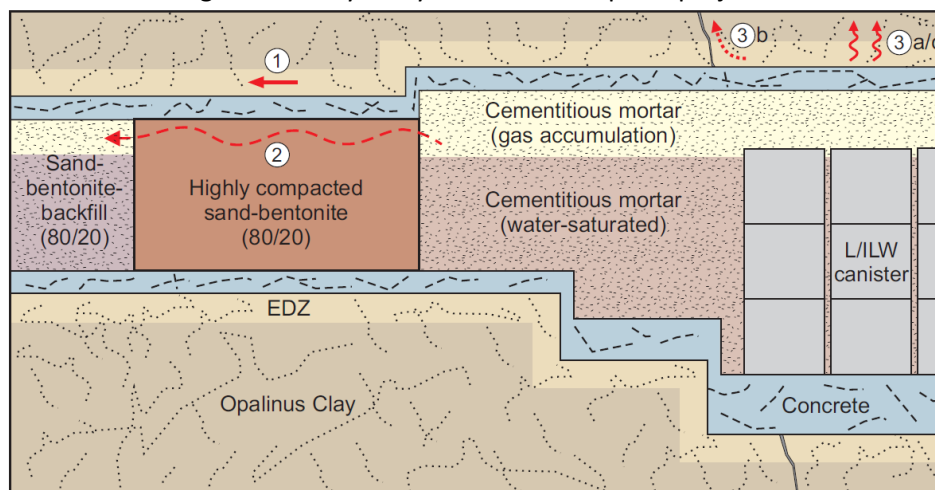
Fig. 1: Schematic description of gas transport in a radioactive waste disposal (NAGRA 2008)

Gas transport in argillaceous rock can be described phenomenologically by four mechanisms from hydraulic and mechanical perspectives (Fig. 2) according to current understanding.
1) Under low gas pressure, the gas transport process is controlled by diffusion and advection of dissolved gas in pore water.
2) When gas pressure exceeds the appeared gas entry pressure of the rock, gas begins to displace pore water and the two-phase flow process dominates the gas transport. The transport capacity of two-phase flow is several orders of magnitudes higher than the transport capacity of dissolved gases (Schlömer & Krooss 1997).
3) If gas pressure exceeds the critical level, the pathway dilatancy controlled gas migration will occur. Due to the low tensile strength of argillaceous rock, micro-cracks can be generated and the permeability will be significantly increased.
4) If gas pressure keeps on increasing, macroscopic fractures can appear. In this case, the gas transport through macro fractures becomes a single-phase flow process.
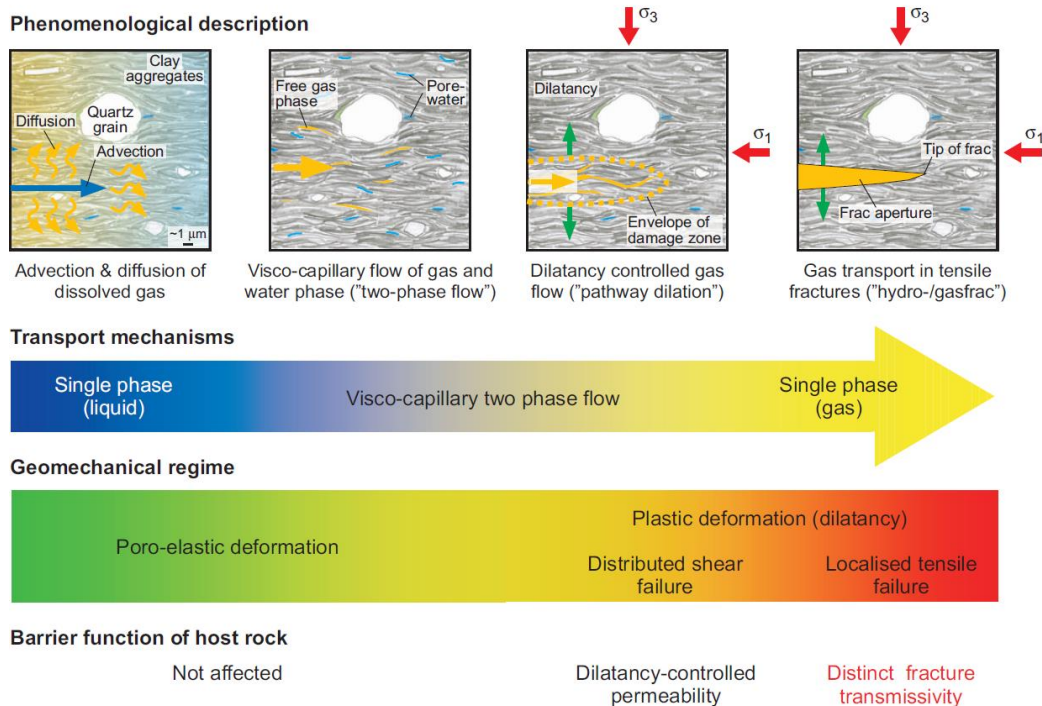
Fig. 2: Classification and analysis of gas transport processes in Opalinus Clay (NAGRA 2008).

This thesis focuses on the two-phase flow controlled and the dilatancy controlled gas transport process in argillaceous rock. A multiphase-flow and mechanical coupled (H^2M) numerical model is developed to investigate gas injection tests with different scales (laboratory, in-situ borehole and in-situ tunnel). The test measured data and observed phenomena are studied and interpreted using the numerical method.

1.2 State of the art

Over the last decade, several laboratory tests looking at gas transport behaviour in argillaceous rock have been carried out (e.g. Boisson et al. 2001, Zhang & Rothfuchs 2004, Marschall et al. 2005, Davy et al. 2007, Popp et al. 2007 and Yang et al. 2010)for the estimate of rock specimen permeability. The gas threshold pressure tests have been studied by Croisé et al. (2006) and Marschall et al. (2003) in the Mont Terri Rock Laboratory. Another in-situ borehole gas migration experiment has been also performed by Shao & Schuster (2009) to investigate the hydraulic properties of Opalinus Clay at different gas pressures. Only few large-scale gas injection tests have been performed to investigate the gas migration processes during the closure phase of a nuclear waste disposal repository. For example, a Gas Migration Test (GMT) at the Grimsel Site in Switzerland was designed to investigate the gas transport through the engineered barrier system (Vomvoris et al. 2002, Senger et al. 2008) and the HG-A test was performed in the Mont Terri Rock Laboratory (Marschall et al. 2006 and Tsang et al. 2012) to study the hydraulic flow pathway around the microtunnel through the sealed section.

The Opalinus Clay is a sediment rock consisting of fine mud particles. The clay minerals content is between 40-80% (Thury and Bossart 1999). The permeability of the Opalinus is extremely low. The deduced permeability from laboratory and in-sit measurement is about 10^{-20} m^2. Thus, the Opalinus Clay is considered as a potential geological formation for radioactive waste final disposal. The properties of Opalinus Clay bas been intensively studied over last fifteen years. The most important physical parameters are presented in the review work by Bock (2009). It has to be noted that the Opalinus Clay has strong anisotropically hydraulic, mechanic and thermal behaviours. In this thesis a

special attention has been paid to consider the most important anisotropic behaviours of the Opalinus Clay by a coupled hydro-mechanical model.

Analyse of coupled processes in porous and fractured medium is needed to research the complicated multifield problem. The concept of coupled processes in geo-system has been comprehensively presented in the publications by Stephansson et al. (2004) and Kolditz et al. (2012a). The coupled thermal-hydro-mechanical processes becomes more and more important to understand many different geotechnical applications, such as radioactive waste disposal (Jing et al. 1995, Hudson et al. 2001, Hou & Lux 2004), geothermal engineering (Watanabe et al. 2009, Zhou & Hou 2013) and CO_2 storage (Kühn et al. 2012, Hou et al. 2012). To advance the understanding and modelling concept of THM processes in geological systems some research projects are set up, e.g. the international research collaboration DECOVALEX, which is initiated in 1992 (Tsang et al. 2009). Based on the coupled THM processes concept different computer codes have been developed and applied, such as CodeBright (Saaltink et al. 2005, Guimaraes et al. 2007), FRT-THM (Liu et al. 2006), ROCMAS (Noorishad & Tsang 1996), TOUGH-FLAC (Rutqvist & Tsang 2003), RockFlow (Kolditz et al. 2003), OpenGeoSys (OGS) (Kolditz et al. 2012b) and THAMES (Ohnishi et al. 1987). Some of those codes have been used for investigating and interpretation the gas injection experiments. Most simulations were done without considering the interactions between hydraulic and mechanical processes. Gas injection tests were simulated using only a two-phase flow model with a modification for the permeability change, which was dependent on gas pressure (Senger et al. 2006). In only a few studies have the mechanical processes been involved and the permeability changed based on the mechanical influence, e.g. by Alonso et al. (2006) and Olivella & Alonso (2008). In their H^2M coupled model the permeability increase was induced by fracture opening, which was calculated by deformation process. In this work a coupled multi-phase flow and mechanical model is introduced, which takes the permeability change and material anisotropy into consideration.

1.3 Dissertation structure

This thesis is structured in the following. Chapter 2 introduces the gas injection tests at different scales (laboratory, in-situ borehole and in-situ tunnel). Chapter 3 descripts the mathematical formation and governing equation of the numerical model. Chapter 4 demonstrates application of the numerical model. In Chapter 5 summary and suggest for the future work are given. Publications produced by this work are listed at the end.

2. Gas injection experiments at different scales

2.1 Laboratory gas injection tests

Two laboratory gas injection tests were performed in IfG (Instituve für Gebirgsmechanik, Germany). The specimens were from the Mont Terri Rock Laboratory in Switzerland. Fig. 3 is a sketch of the experiment concept for gas injectio. A cylinder specimen with 150.45 mm height and 73.59 mm diameter was prepared. Two boreholes with 30 mm length and 4 mm diameter were drilled at the top and the bottom surface. Nitrogen was injected from the bottom borehole. The out-flow and the rate from the borehole at the top surface was measured under atmospheric pressure. The cylinder specimen was sealed with a rubber jacket under hydrostatical loading condition (axial loading is same as confining pressure).
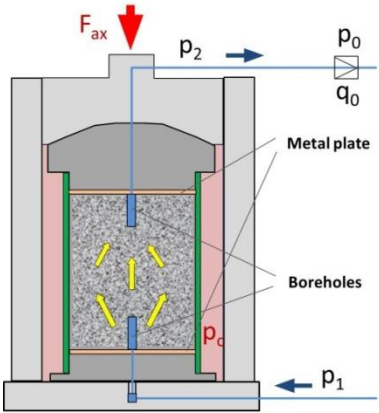
Fig. 3: Sketch of the laboratory experiment (Popp et al. 2007)

Two laboratory gas injection tests are presented in this chapter. One was loading cycle test (Fig. 4), which had two test stages. At the beginning the confining pressure was constant at 1 MPa, and gas injection pressure was increased stepwise from 0.1 MPa to 0.9 MPa. With the increased gas injection pressure the measured gas out-flow rate was synchronously increased. After the gas injection pressure reached 0.9 MPa the confining pressure started to raise step by step and had an end level of 5 MPa. Inversely, the gas out-flow rate dropped with the increased confining pressure, which indicated decrease of the permeability due to the compression.
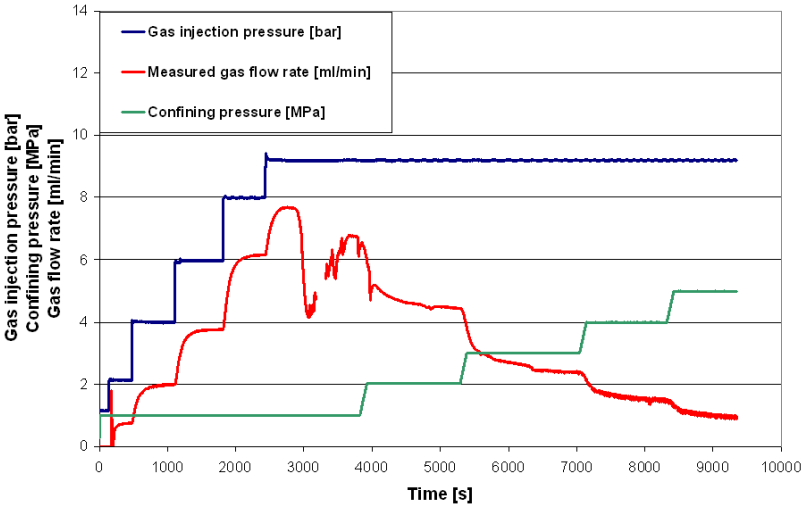
Fig. 4: Measured data of the loading cycle test (Popp et al. 2007)

The other test was fracture cycle test (Fig. 5), by which the confining pressure kept constant at 3 MPa. Gas pressure was increased from 1 MPa to 3.5 MPa, which is higher than the confining pressure. The gas out-flow was measured when the injection pressure was 2 MPa and was increased slightly with the injection pressure. When the gas injection pressure reached 3.5 MPa, significant increase of the gas out-flow rate was measured. A possible explanation was the remarkable permeability increase due to the generation of micro-cracks. At the end of the test the gas injection pressure dropped to 1 MPa, and the gas out-flow rate was decreased.
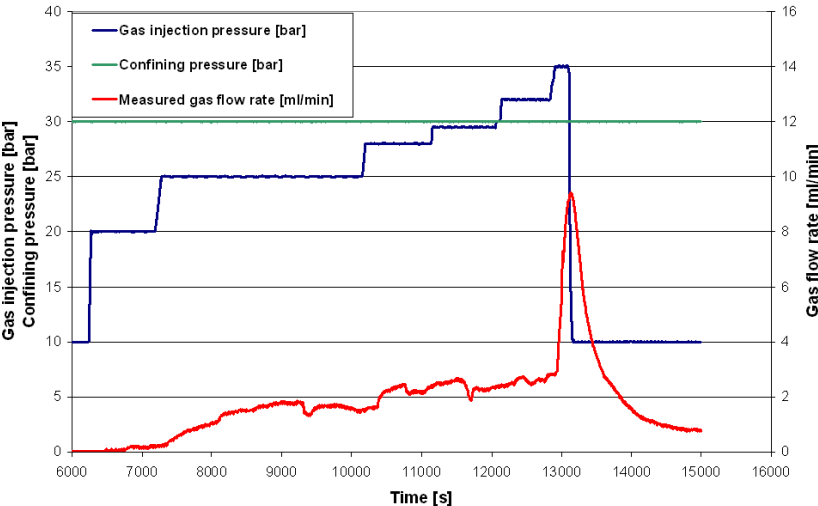
Fig. 5: Measured data of the fracture cycle test (Popp et al. 2007)

2.2 In-situ borehole tests

Gas injection tests in the Mont Terri Rock Laboratory were conducted within the framework of the HG-B experiment, which aimed at determining gas permeability in saturated Opalinus Clay and the hydraulic characterisation of the tunnel near field (Shao & Schuster, 2009). In the EZ-A niche (Fig. 6, left), an experiment was carried out to investigate the pathway dilatancy controlled gas migration in Opalinus Clay under in-situ conditions (Fig. 6, right). Four parallel boreholes (BHG-B6 to BHG-B9) were drilled using the air-drilling technique, each with a diameter of 86 mm. BHG-B6, -B7 and –B8 had the same distance (0.5 m) to BHG-B9 (Fig. 7, left). All boreholes were perpendicular to the bedding planes and oriented 45° upwards (Fig. 7, right). The central 10 m long borehole (BHG-B9) was injection borehole, and the last one-meter-section was used as the test section, which was sealed with a 0.6 m long packer.
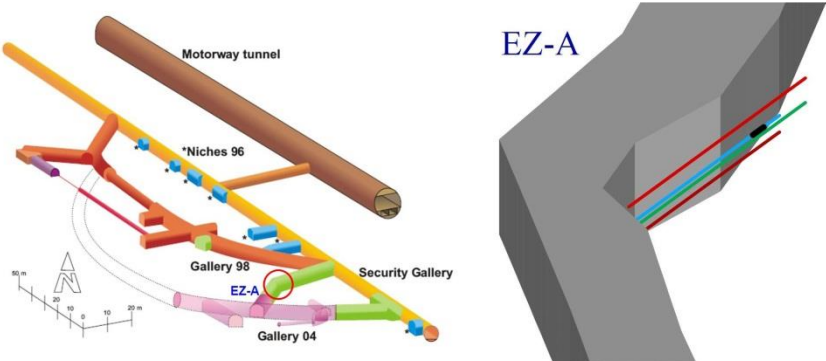
Fig. 6: Mont Terri Rock Laboratory (left) and location of the boreholes for the in-situ experiment (right)
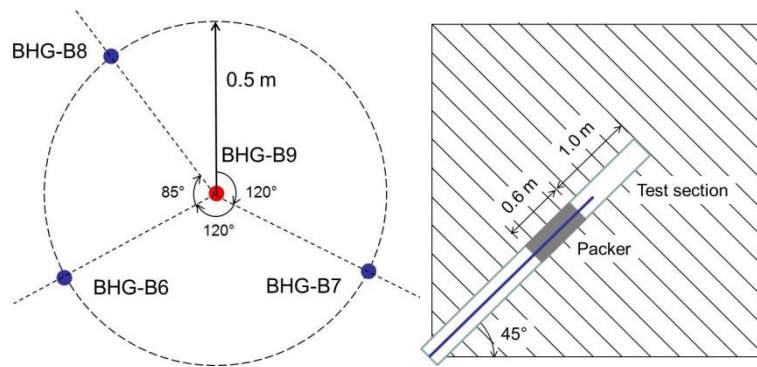
Fig. 7: Layout of the boreholes (left) and sketch of the test and packer section

Pulse tests with a stepwise increase of gas injection pressure were performed in BHG-B9 test section, which is located outside of the excavation damaged zone (EDZ) of the EZ-A niche. In total, three series of gas injection tests and two series of formation water injection tests were carried out (Fig. 8). Every series included several tests with stepwise increased gas/water injection pressure. After the shut-off of the injection line, the interval pressure was monitored. In this thesis we focus on the first serie of the gas injeciton test.
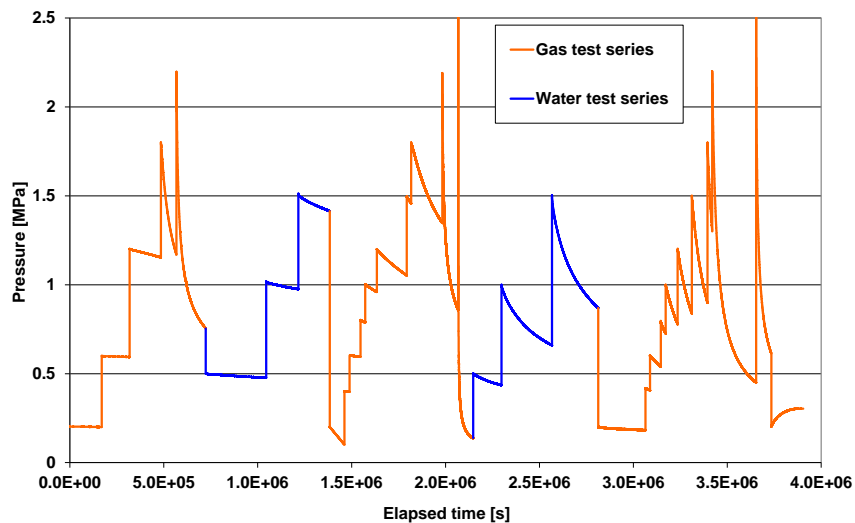
Fig. 8: Gas and water injection series (Shao and Schuster 2009)

2.3 In-situ micro tunnel tests

To investigate the gas/water flow path through the EDZ around the sealing section, series in-situ injection tests were carried out in HG-A location in the Mont Terri Rock Laboratory. The HG-A tunnel is located in Gallery 04 (Fig. 9 (left)) with a length of 13 m diameter of 1 m. Details of the HG-A tunnel is shown in Fig. 9 (right). The section between 10 - 13 m was used for injection tests. The test section was refilled with quartz gravel to reduce the water injection supply requirement. A megapacker was emplaced in the tunnel section between 6-10 m to seal the test section. The 1 m gap between the mega packer and the test section was backfilled with cement injection to seal the whole sealing section. Steel liner has been installed from the tunnel entrance to 6 m. Sepcial attention will be paid in this thesis on the measurement of the piezometer in the megapacker section to investigate the flow paths around the tunnel. Piezometers were emplaced to measure the pore water pressure of three section of the megapacker (PES1, PES2 and

6

PES3). In each measuremetn section, four piezometers were set at 3, 6, 9 and 12 o'clock positions (Fig. 9 (right)) (view direction from tunnel entrance to the rear end).
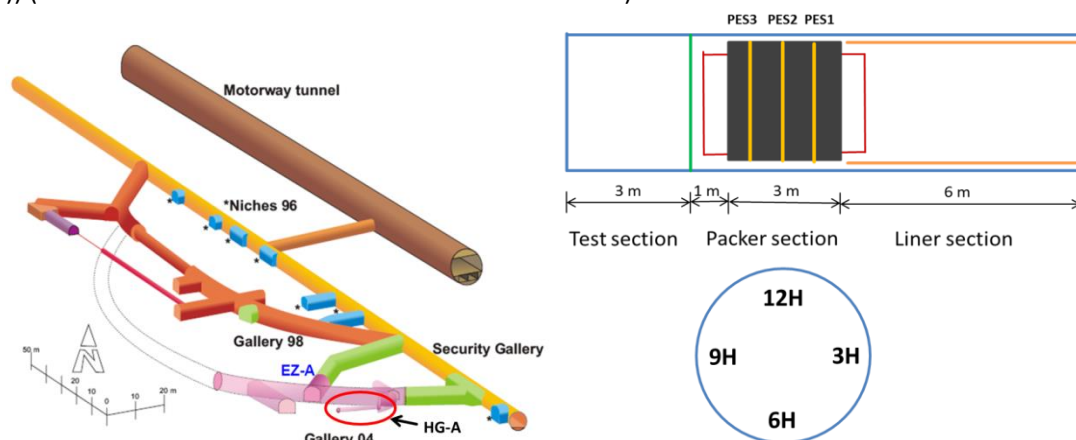
Fig. 9: Location of HG-A experiment (left) and test, packer and liner sections of the HG-A tunnel and the piezometer location in the packer section (right) (EP3)

The HG-A micro tunnel was drilled in Febuary 2005. The drilling direciton was horizontal and parallel to the bedding plane strike direction. The bedding plane was 45° oblique. The average drilling speed was about 1.5 m/d and the tunnel wall was relative stable during the drilling operation. After the drillign same breakouts took place in 3 and 10.5 o'clock positions. The breakout areas were considered as potential flow paths with high permeability.

The measurement of pressure in test section and megapacker section are shown in Fig. 10 with the registred water and gas flow reate. The water injection tests started after resaturaion of the test section. Two types tests were carried out, shut-in test and constant injection rate test. During the shut-in test, the pressure in the test section was increased rapidly with the high injetion rate. The pressure recovery was measured after the injection shut-off. During the constant constant injection rate tests, different injection rates between 0.1 and 10 ml/min were applied. The research work by Lanyon et al. 2007 analysed the permeability variation during the HG-A water injection tests. It indicated that the flow paths around the seal were partly sealed, with the decreased permeability resulting from the long-term resaturation of the rock.

Since Febuary 2010 the gas injection tests started and nitrogen was injected through the middle port on the tunnel ceiling. Until now three gas injection series were performed.

First gas injection phase: The gas injection rate was 20 mlN/min at the beginning. When the pressure in the test section reached about 1.2 MPa, the injection rate was decreased and was cotrolled to keep the pressure relatively constant at 1.2 MPa. The gas injection rate varied between 5-15 mlN/min. After two months, gas injection was stopped and the pressure recovery from 1.2 to 0.8 MPa in the test section was registered.

Second gas injection phase: The second gas injection phase was planned with a constant gas injection rate of 10 mlN/min. Due to an in-situ power failure the injection rate was dropped to 8.6 mlN/min for 24 days and then to 5.7 mlN/min for 6 days of the test. The pressure in the test section was increased with the constant gas injection rate from the beginning. When the pressure reached ca. 1.35 MPa, a pressure breakdown was observed. After that the pressure was decreased to 1 MPa and remained constant. Same as the first gas injection test, pressure recovery after the injection shut-off was measured.

Third gas injection phase: During the third gas injection phase the injection rate was kept constant at 20 mlN/min. The pressure was increased faster than it had been in the second gas injection phase, because of the injection rate being twice as high. However, it was slower than in the first gas test, which had the

same injection rate of 20 mlN/min. Finnaly, the injection rate was twice as high as in the second gas injection phase, but the pressure remained at the same level. This observation suggests that permeability had increased irreversibly during the breakdown of the third gas injection phase. More details of the gas injection tests can be found in EP3.
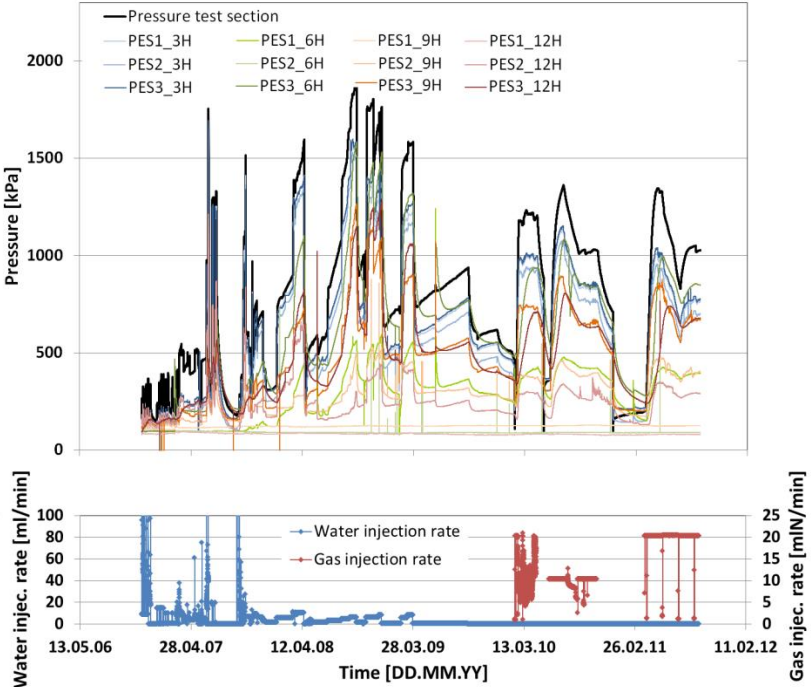

Fig. 10: Pressure measured throughout the period in the test and packer sections, with water and gas injection rates

3. Mathematical and numerical model

A coupled multi-phase flow and mechanical (H^2M) model was developed to simulate the gas injection tests. The porous medium is assumed to be homogenous and continuum, which consisting of three phases, liquid, gas and solid. The capillary pressure, gas pressure and solid displacement are set as primary variables. The numerical model has been implemented in the scientific computer code OpenGeoSys (OGS) and is introduced in this chapter.

3.1 Hydraulic process

3.1.1   Mass balance equations

The water and gas flows in the deformable porous medium are considered. Generally, the mass balance equation of each phase is expressed as (Helmig 1997, Kolditz et al. 2012a)

$$\frac{\partial n \rho^\pi S_\pi}{\partial t} + \rho^\pi S_\pi \nabla \frac{\partial \mathbf{u}}{\partial t} + \nabla \mathbf{q}^\pi = 0 \tag{1}$$

where, n is the porosity, ρ^π is the density, S^π is the saturation and q^π is the velocity of the phase π, $\mathbf{u}$ is the displacement. Considering that the hydraulic primary variables of this numerical model (capillary pressure (p^c) and gas pressure (p^g)), the mass balance equations of the water and gas phase are expressed as:

$$n\rho^w \frac{\partial S_w}{\partial p^c} \frac{\partial p^c}{\partial t} + \rho^w S_w \nabla \frac{\partial \mathbf{u}}{\partial t} + \nabla \mathbf{q}^w = 0 \tag{2}$$

$$-n\rho^g \frac{\partial S_w}{\partial p^c} \frac{\partial p^c}{\partial t} + n(1-S_w)\rho^g \frac{\partial \rho^g}{\partial p^g} \frac{\partial p^g}{\partial t} + \rho^g (1-S_w)\nabla \frac{\partial \mathbf{u}}{\partial t} + \nabla \mathbf{q}^g = 0 \tag{3}$$

3.1.2   Constitutive equations

Capillary pressure is defined by the sorption equilibrium equation (Sanavia et al., 2006) as:

$$p^c = p^g - p^w \tag{4}$$

The phase flux q^π in Eq. (1) can be expressed with capillary pressure and gas pressure and defined by modified Darcy's law (Kolditz et al. 2012a) as:

$$\mathbf{q}^w = -\rho^w \frac{\mathbf{k}^{int} k^{r,w}}{\mu^w} \left(\nabla p^g - \nabla p^c + \rho^w \mathbf{g} \right) \tag{5}$$

$$\mathbf{q}^g = -\rho^g \frac{\mathbf{k}^{int} k^{r,g}}{\mu^g} \left(\nabla p^g + \rho^g \mathbf{g} \right) \tag{6}$$

where $\mathbf{k}^{ini}$ is the intrinsic permeability tensor, μ^π is the viscosity and $k^{r,\pi}$ is the relative permeability of water and gas phase.

The relative permeability of the water and gas phases is described by the Mualem approach (Kolditz et al. 2012a, Wang et al. 2011; Helmig 1997) having the following form:

$$k^{r,g} = \left(1-S_e\right)^{\frac{1}{2}} \left(1-S_e^{\frac{m}{m-1}}\right)^{2(1-1/m)} \tag{7}$$

$$k^{r,w} = S_e^{\frac{1}{2}} \left[1-\left(1-S_e^{\frac{m}{m-1}}\right)^{\frac{m-1}{m}}\right]^2 \tag{8}$$

The van Genuchten model is applied to describe the relationship between water saturation and capillary pressure as (van Genuchten 1980):

$$p^c = p_0 \left(S_e^{\frac{m}{1-m}} - 1\right)^{\frac{1}{m}} \tag{9}$$

where p_0 is the gas entry pressure, m is the shape factor and S_e is the effective saturation, which is calculated as:

$$S_e = \frac{S_w - S_{wr}}{1 - S_{wr} - S_{gr}} \tag{10}$$

where, S_{wr} and S_{gr} are the residual saturation of the water and gas phases respectively.

3.1.3   Permeability modification approaches

Permeability variation during the gas injection tests is one of the most imprtant issue, which has great impact on the gas transport in porouse medium. Two approches are developed by the author to consider the intrinsic permeability change in the coupled H^{2}M model (EP1, EP2).

1) Gas pressure dependent approach: In this appoach a critical value (p_{thr}) is introduced as a criterion for the high and low gas pressure. For simplicity, linear dependence is applied. Based on the laboratory and in-situ observation the permeability increases slightly if gas pressure is lower than the threshold value and increases rapidly when gas pressure exceeds the critical value. This assumption is considered from two perspectives: 1) If gas pressure is lower than a critical value, the change of gas pressure can only cause extension or compaction of pore space, which has limited effect on permeability; 2）if gas pressure exceeds the critical threshold level, micro-cracks are generated and the permeability increases significantly due to connection and propagation of micro-cracks. This permeability modification approach can be expressed as:

$$\mathbf{k} = f\left(p_g\right)\mathbf{k}_{int}^{ini} = \begin{cases} \left(1+a_1 p_g\right)\mathbf{k}_{int}^{ini} & , \quad p_g \le p_{thr}[\text{MPa}] \\ \left(a_2\left(p_g - p_{thr}\right)+1+a_1 p_{thr}\right)\mathbf{k}_{int}^{ini} & , \quad p_g > p_{thr}[\text{MPa}] \end{cases} \tag{11}$$

2) Deformation depent appoach: In this appoach the permeability is controlled by the deformation process, and takes the following two aspects into consideration: a) As long as the plastic strain has not appeared the permeability change is only dependent on the change of pore space induced by elastic volumetric deformation; b) If plastic strain occurs, significant increase in the permeability is considered as the generation and opening of micro-cracks induced by gas pressure. The deformation dependent permeability approach can be expressed as:

$$\mathbf{k} = f\left(\Delta\varepsilon_{vol}\right)e^{b_1\Delta\bar{\varepsilon}^p}\mathbf{k}_{int}^{ini} \tag{12}$$

with,

$$f\left(\Delta\varepsilon_{vol}\right)=\begin{cases}10^{b_2\Delta\varepsilon_{vol}} & , \quad compaction \\ 10^{b_3\Delta\varepsilon_{vol}} & , \quad extension\end{cases}$$

(13)

Permeability changes behaviour compaction and extension can be defined respectively (Eq. (13)) based on some laboratory and in-situ observations.

3.2 Deformation equations

3.2.1 Effective stress concept

The Bischof effective stress concept of the unsaturated porous medium takes the saturation and pressure of each phase into account and has the form as (Kolditz et al. 2012a, Wang et al. 2007):

$$\boldsymbol{\sigma}' = \boldsymbol{\sigma} + \alpha\sum S_\pi p^\pi \mathbf{I}$$

(14)

Considering the primary variables of the model are capillary pressure (p^c) and gas pressure (p^g), the effective stress tensor $\boldsymbol{\sigma}'$ can be expressed as:

$$\boldsymbol{\sigma}' = \boldsymbol{\sigma} + \alpha(p^g - S_w p^c)\mathbf{I}$$

(15)

where, α is Biot's coefficient and $\mathbf{I}$ is the unit tensor.

3.2.2 Momentum balance equations

The momentum balance equation in terms of effective stress (Sanavia et al., 2006; Wang et al., 2011), can be expressed as:

$$\nabla\left(\boldsymbol{\sigma}' - \alpha\left(p^g - S_w p^c\right)\mathbf{I}\right) + \rho\mathbf{g} = 0$$

(16)

where σ' is the effective stress tensor, α is the Biot coefficient, ρ is the density of the porous medium or as

$$\rho = \left(1-n\right)\rho^s + nS_w\rho^w + n\left(1-S_w\right)\rho^g$$

(17)

3.2.3 Constitutive equations

The elastic-perfectly plastic constituvie law is applied for the stress-strain behaviour. When the stress state doesn't excced the yield limit, the stress-strain behavior is pure elastic, and can be expressed using the generlizied Hooke's law for anisotropic material as:

$$d\boldsymbol{\varepsilon} = (\mathbf{D}^e)^{-1}d\boldsymbol{\sigma}$$

(18)

where, $(\mathbf{D}^e)^{-1}$ has the form as:

$$(\mathbf{D}^e)^{-1} = \begin{bmatrix} 1/E_{//} & -\upsilon_{////}/E_{//} & -\upsilon_{//\perp}/E_\perp & & & \\ -\upsilon_{////}/E_{//} & 1/E_{//} & -\upsilon_{//\perp}/E_\perp & & & \\ -\upsilon_{\perp//}/E_{//} & -\upsilon_{\perp//}/E_{//} & 1/E_\perp & & & \\ & & & 1/2G_{////} & & \\ & & & & 1/2G_{//\perp} & \\ & & & & & 1/2G_{//\perp} \end{bmatrix}$$

(19)

where, $E_{//}$ and $E_{//}$ are Young's moduli in the bedding plane, $E_{\perp}$ is in the direction normal to the bedding plane. $v_{\perp//}$, $v_{//\perp}$ and $v_{////}$ are the Poisson ratios in the bedding plane and the anisotropic direction, respectively.

The plasticity is calclated with the return mapping algorithm when the stress state excceds the yield limit. Using the classic return mapping methode the stress invrement is calculated as (Crisfield 1997, Clausen 2007):

$$\Delta\sigma_{ij} = \Delta\sigma_{ij}{}^{e} - \Delta\sigma_{ij}{}^{P} = D_{ijkl}{}^{e}\left(\Delta\varepsilon_{ij} - \lambda\frac{\partial G}{\partial\sigma ij}\right) \tag{20}$$

with

$$\lambda = \frac{\left(\partial F/\partial\sigma_{ij}\right)^{T} D_{ijkl}{}^{e}\Delta\varepsilon_{kl}}{\left(\partial F/\partial\sigma_{ij}\right)^{T} D_{ijkl}{}^{e}\left(\partial G/\partial\sigma_{kl}\right)} \tag{21}$$

where, F is the yield function, G is the potential function and has the similar form as the yield fuction (F) by associate flow rule.

The yield function can be defined according to different concept, e.g. Drucker-Prager model or Mohr-Coloumb model:

Drucker-Prager
$$F^{s} = \alpha_{\theta}I_{1} + \sqrt{J_{2}} - k_{\theta}$$
$$F^{t} = \frac{1}{3}I_{1} - \sigma^{t} \tag{22}$$

Mohr-Coloumb
$$F^{s} = \frac{1}{3}(N_{\phi}-1)I_{1} + \frac{2}{3}(N_{\phi}\sin(\theta+\frac{2}{3}\pi) - \sin(\theta-\frac{2}{3}\pi))\sqrt{J_{2}} - f_{c}$$
$$F^{t} = \frac{1}{3}I_{1} + \frac{2}{\sqrt{3}}\sqrt{J_{2}}\cos\theta - \sigma^{t} \tag{23}$$

F^{s} and F^{t} are yield functions of shear and tensile criterion, respectively. I_{1} and J_{2} are stress invariants. α_{θ} and k_{θ} are material parameters, which can be defined with the inner adjustment of Mohr-Coulomb pyramid (Itasca, 2009). σ^{t} is tensile strength and f_{c} is uniaxial compression strength. θ is the lode angle and N_{ϕ} is defined as:

$$N_{\phi} = \frac{1+\sin\phi}{1-\sin\phi} \tag{24}$$

The term of $\partial F/\partial\sigma_{ij}$ in Eq. 19 can be expressed in a general form as:

$$\frac{\partial F}{\partial\sigma_{ij}} = \frac{\partial F}{\partial I_{1}}\frac{\partial I_{1}}{\partial\sigma_{ij}} + \frac{\partial F}{\partial J_{2}}\frac{\partial J_{2}}{\partial\sigma_{ij}} + \frac{\partial F}{\partial\theta}\frac{\partial\theta}{\partial\sigma_{ij}} \tag{25}$$

The derivatives of stress invariants (I_{1}, J_{2}) and lode angle (θ) is well-known and can be found in Pietruszczak et al. (2002) in form as:

$$\frac{\partial I_{1}}{\partial\sigma_{ij}} = -\delta_{ij} \quad ; \quad \frac{\partial J_{2}}{\partial\sigma_{ij}} = s_{ij} \quad ; \quad \frac{\partial\theta}{\partial\sigma_{ij}} = \frac{\sqrt{3}}{2\sqrt{J_{2}}^{3}\cos 3\theta}\left(\frac{3J_{3}}{2J_{2}}s_{ij} - s_{ik}s_{kl} + \frac{2}{3}\sqrt{J_{2}}\delta_{ij}\right) \tag{26}$$

where, δ_{ij} is Kronecker delta, s_{ij} is deviatoric stress tensor, J_{3} is the third deviatoric stress

12

invariant.

The anisotropic strength behaviour dependents on the loading direction and the bedding plane orientation. Thus, the conventional plastic model is extended. The anisotropic plasticity is modelled using the micro-structure tensor method, which was first presented by Pietruszczak & Mroz (2000, 2001). Since then some studies (Pietruszczak et al. 2002; Lydzba et al. 2003) have been done using the micro structure method to model laboratory rock strength tests.

A two-order tensor a_{ij} was introduced as a measure of material fabric. a_1, a_2 and a_3 are the three principal values of the microstructure tensor. The indices 1, 2, 3 indicate the principal directions of the anisotropic material. The traction moduli on the planes normal to the material principal axes are defined as:

$$L_i = (\sigma_{i1}^2 + \sigma_{i2}^2 + \sigma_{i3}^2)^{1/2}, \qquad i = 1, 2, 3 \tag{27}$$

A loading vector l is defined as:

$$l_i = \frac{L_i}{\left(L_1^2 + L_2^2 + L_3^2\right)^{1/2}}, \qquad i = 1, 2, 3 \tag{28}$$

Then, a scalar variable η can be expressed as:

$$\eta = a_{ij} l_i l_j \tag{29}$$

The variable η specifies the effect of loading on the anisotropic material structure. For example, the three principal values of the microstructure tensor are given as $a_1 = a_2 = 1$ and $a_3 = 0.5$. The index 1 and 2 indicate the principal direction in the bedding plane, and index 3 is the direction perpendicular to the beddign plane. Considering a uniaxial loading case β is the angle between the loading axes and the bedding-normal direction. Fig. 11 shows the relationship between the scalar variable η and the loading direction β. Now the relationship between the loading direction and the dedding plan orientation can be describted by the introduced variable η.
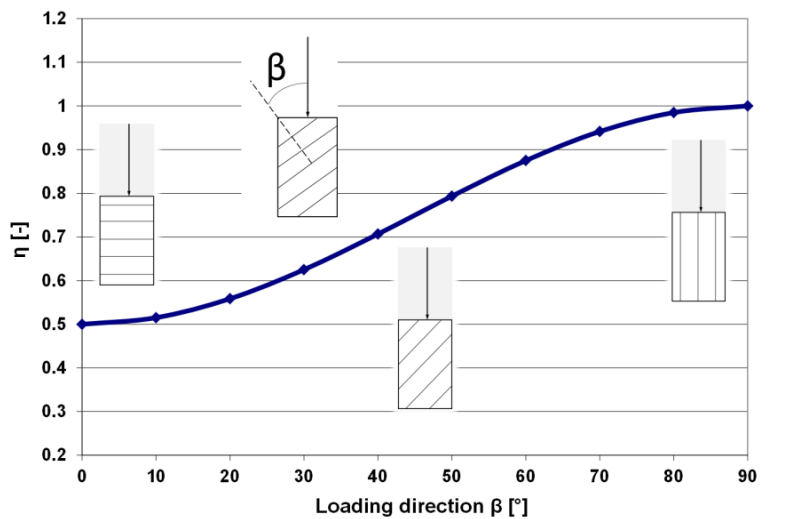

Fig. 11: Variation of η whit loading direction (EP3)

According to the research work by Naumann (2007) and Gräsle & Plischke (2010), the uniaxial compression strength of Opalinus Clay varies with the loading direction, although the internal friction angle does not change significantly. Using the laboratory measurement of triaxial tests, the uniaxial strength under different loading directions can be derived. If the Mohr-Coulomb criterion is applied, since the parameter η is introduced, the varied uniaxial strength f_c can be described as a function of η in a general form:

$$f_c(\eta) = b_0 + b_1\eta + b_2\eta^2 + b_3\eta^3 + b_4\eta^4 + \ldots \tag{30}$$

Parameter b_i can be estimated by fitting the laboratory measurement. Fig. 7 shows the fitted $f_c(\eta)$ with b_0=70820400, b_1=-171383200 and b_2=113588800. The parameter sets were used for the numerical simulation in Chapter 4.
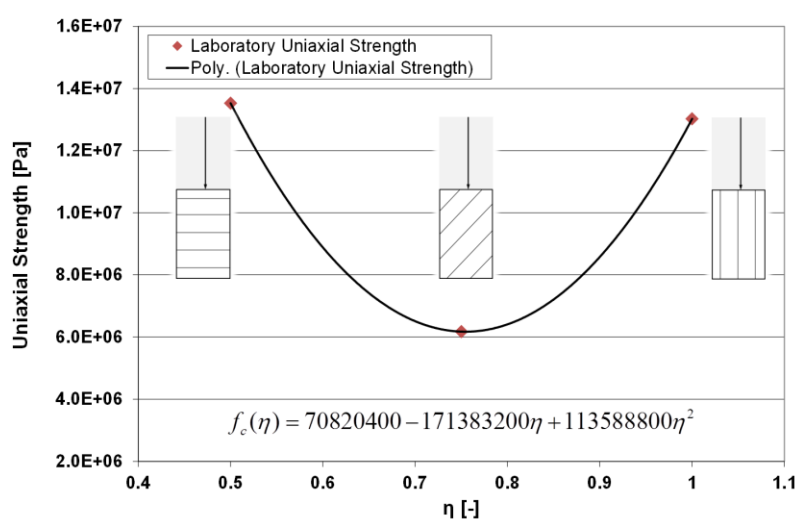

Fig. 12: Relationship between uniaxial strength and loading direction parameter η

Since uniaxial strength (f_c) is not constant and dependent on the loading direction, eq. (25) can be extended in form as:

$$\frac{\partial F}{\partial \sigma_{ij}} = \frac{\partial F}{\partial I_1}\frac{\partial I_1}{\partial \sigma_{ij}} + \frac{\partial F}{\partial J_2}\frac{\partial J_2}{\partial \sigma_{ij}} + \frac{\partial F}{\partial \theta}\frac{\partial \theta}{\partial \sigma_{ij}} + \frac{\partial F}{\partial f_c}\frac{\partial f_c}{\partial \eta}\frac{\partial \eta}{\partial \sigma_{ij}} \tag{31}$$

The term of $\partial\eta/\partial\sigma$ can be expressed as (Pietruszczak et al. 2002):

$$\frac{\partial \eta}{\partial \sigma} = \frac{2(a_{ki}\sigma_{kj}\sigma_{pq}\sigma_{pq} - a_{pk}\sigma_{pq}\sigma_{kq}\sigma_{ij})}{(\sigma_{mn}\sigma_{mn})^2} \tag{32}$$

To this end, an elasto-plastic model with the micro tensor method was thus developed and the parameters for η were also estimated based on the laboratory measurements.

3.3 Finite element formulation

Finite element method is used in OGS for solving complicated thermo-hydro-mechanical-chemical coupling problems (Kolditz et al. 2012b). The method of weighted residuals is applied to derive the weak formulation of the balance equations for water/gas flow and deformation (Lewis and Schrefler, 1998; Kolditz et al. 2012b), and can be written as:

Water flow

$$\int_\Omega n\rho^w \frac{\partial S_w}{\partial p^c}\frac{\partial p^c}{\partial t}\omega d\Omega + \int_\Omega \rho^w S_w \frac{\partial}{\partial t}(\nabla\cdot\mathbf{u})\omega d\Omega + \int_\Omega \mathbf{q}^w\cdot\nabla\omega d\Omega + \int_\Gamma \mathbf{q}^w\mathbf{n}\omega d\Gamma = 0 \tag{33}$$

Gas flow

$$-\int_\Omega n\rho^g \frac{\partial S_w}{\partial p^c}\frac{\partial p^c}{\partial t}\omega d\Omega + \int_\Omega n(1-S_w)\rho^g \frac{\partial \rho^g}{\partial p^g}\frac{\partial p^g}{\partial t}\omega d\Omega$$

$$+\int \rho^g(1-S_w)\frac{\partial}{\partial t}(\nabla\cdot\mathbf{u})\omega d\Omega + \int_\Omega \mathbf{q}^g\cdot\nabla\omega d\Omega + \int_\Gamma \mathbf{q}^g\mathbf{n}\omega d\Gamma = 0$$

(34)

Deformation

$$\int_\Omega \frac{1}{2}(\boldsymbol{\sigma}' - \alpha(p^g - S_w p^c)\mathbf{I}):(\nabla\boldsymbol{\omega}+(\nabla\boldsymbol{\omega})^\mathrm{T})d\Omega + \int_\Omega \boldsymbol{\omega}^\mathrm{T}\cdot\rho\mathbf{g}d\Omega - \int_\Gamma \boldsymbol{\omega}^\mathrm{T}\cdot\mathbf{t}d\Gamma = 0 \qquad (35)$$

Here Ω and Γ denote the model domain and domain boundary respectively. $\omega\in v^1\subset H_\Gamma^1(\Omega)^1$ is the linear function, and $\omega\in v^n\subset H_\Gamma^n(\Omega)^n$ is the quadratic test function in n-dimensional space (Wang et al. 2009). All primary variables (p^c, p^g and $\mathbf{u}$) are approximated by admissible interpolation functions in the Tylor-Hood finite element space. To discretize the weak forms of the balance equations, a Galerkin method is used. The finite element formulation of the H²M problem can be written in matrix form as:

$$\begin{bmatrix}\mathbf{M}_{cc} & \mathbf{M}_{cg}\\ \mathbf{M}_{gc} & \mathbf{M}_{gg}\end{bmatrix}\frac{\partial}{\partial t}\begin{bmatrix}\mathbf{p}^c\\ \mathbf{p}^g\end{bmatrix} + \begin{bmatrix}\mathbf{K}_{cc} & \mathbf{K}_{cg}\\ \mathbf{K}_{gc} & \mathbf{K}_{gg}\end{bmatrix}\begin{bmatrix}\mathbf{p}^c\\ \mathbf{p}^g\end{bmatrix} = \begin{bmatrix}\mathbf{f}_c(\mathbf{u})\\ \mathbf{f}_g(\mathbf{u})\end{bmatrix}$$

$$\mathbf{K}_{uu}\mathbf{u} = \mathbf{f}_u(\mathbf{p}^c,\mathbf{p}^g)$$

(36)

The coupling terms in the balance equations are treated as right-hand side (RHS) terms ($\mathbf{f}_c$, $\mathbf{f}_g$ and $\mathbf{f}_u$). $\mathbf{M}$ and $\mathbf{K}$ are process-specific mass and Laplace matrices, which can be expressed detail as following forms:

$$\mathbf{M}_{cc} = \int_\Omega \mathbf{N}_p^\mathrm{T} n\rho^w \frac{\partial S_w}{\partial p^c}\mathbf{N}_p d\Omega$$

$$\mathbf{M}_{cg} = \mathbf{0}$$

$$\mathbf{M}_{gc} = -\int_\Omega \mathbf{N}_p^\mathrm{T} n\rho^g \frac{\partial S_w}{\partial p^c}\mathbf{N}_p d\Omega$$

$$\mathbf{M}_{gg} = \int_\Omega \mathbf{N}_p^\mathrm{T} n(1-S_w)\rho^g \frac{\partial \rho^g}{\partial p^g}\mathbf{N}_p d\Omega$$

$$\mathbf{K}_{cc} = -\int_\Omega (\nabla\mathbf{N}_p)^\mathrm{T}\rho^w \frac{\mathbf{k}^{int}k^{r,w}}{\mu^w}(-\nabla\mathbf{N}_p)d\Omega$$

$$\mathbf{K}_{cg} = -\int_\Omega (\nabla\mathbf{N}_p)^\mathrm{T}\rho^w \frac{\mathbf{k}^{int}k^{r,w}}{\mu^w}(\nabla\mathbf{N}_p)d\Omega$$

$$\mathbf{K}_{gc} = \mathbf{0}$$

$$\mathbf{K}_{gg} = -\int_\Omega \nabla\mathbf{N}_p^\mathrm{T}\rho^g \frac{\mathbf{k}^{int}k^{r,g}}{\mu^g}\nabla\mathbf{N}_p d\Omega$$

$$\mathbf{f}_c(\mathbf{u}) = \int_\Omega \nabla\mathbf{N}_p^\mathrm{T}[\rho^w \frac{\mathbf{k}^{int}k^{r,w}}{\mu^w}\rho^w\mathbf{g}]d\Omega - \int_\Omega \mathbf{B}^\mathrm{T}\rho^w S^w \mathbf{m}^m\mathbf{N}_p d\Omega\frac{\partial\mathbf{u}}{\partial t} - \int_\Gamma \mathbf{N}_p^\mathrm{T}q^w d\Gamma$$

$$\mathbf{f}_g(\mathbf{u}) = \int_\Omega \nabla\mathbf{N}_p^\mathrm{T}[\rho^g \frac{\mathbf{k}^{int}k^{r,g}}{\mu^g}\rho^g\mathbf{g}]d\Omega - \int_\Omega \mathbf{B}^\mathrm{T}\rho^g(1-S^w)\mathbf{m}^m\mathbf{N}_p d\Omega\frac{\partial\mathbf{u}}{\partial t} - \int_\Gamma \mathbf{N}_p^\mathrm{T}q^g d\Gamma$$

$$\mathbf{K}_{uu} = \int_\Omega \mathbf{B} \mathrm{d}\Omega^{\mathrm{T}} \mathbf{B} \mathbf{D}^{ep}$$

$$\mathbf{f}_u(\mathbf{p}^c, \mathbf{p}^g) = \int_\Omega \mathbf{B}^{\mathrm{T}} \alpha \mathrm{m}^m \mathbf{N}_p \mathrm{d}\Omega \mathbf{p}^g - \int_\Omega \mathbf{B}^{\mathrm{T}} \alpha S^w \mathrm{m}^m \mathbf{N}_p \mathrm{d}\Omega \mathbf{p}^c$$
$$- \int_\Omega \mathbf{N}_u \rho \mathbf{g} \mathrm{d}\Omega + \int_\Gamma \mathbf{N}_u^{\mathrm{T}} \mathrm{t} \mathrm{d}\Gamma$$

(37)

with $\mathbf{N}_p$ and $\mathbf{N}_u$ are the shape functions of capillary/water pressure and displacement. $\mathbf{m}^m = (1,1,1,0,0,0)$ is a mapping vector. $\mathbf{B}$ is the strain-displacement matrix.

4. Model validation and interpretation

4.1 Transient gas flow test

To validate the developed numerical model a pulse test for determination of air permeability in rock is simulated and compared with analytical solution. The test conditions are shown schematically in Fig. 13. The cylinder rock specimen has the initial gas pressure of 101325 Pa.
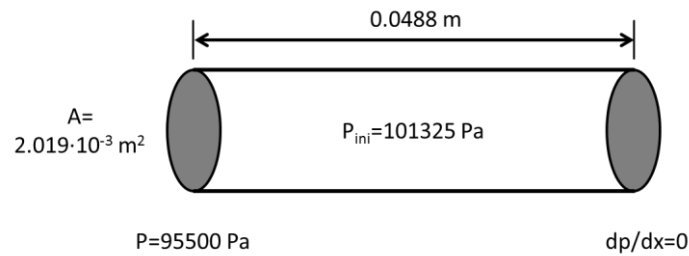

Fig. 13: Schematic description of the transient gas flow in a column

The pressure at the left end keeps constant with 95500 Pa and the other end is closed. All important parameters are listed in Table 1. In this example the rock is assumed homogeneous and isotropic. The gas flow process is isothermal and the gas density obtains the ideal gas law.

Table 1: Rock and gas properties

Parameter	Unit	Value
Rock permeability	m^2	$2.77 \cdot 10^{-19}$
porosity	-	0.005
Gas viscosity	Pa·s	$1.78 \cdot 10^{-5}$
Density of ideal gas at atmospheric pressure	$kg \cdot m^3$	1.225

The gas is extracted from the cylindrical specimen at the one side. The other end was closed with no gas flow. The analytical solution of this unsteady gas flow problem can be found in Kolditz & Zielke (1996). Fig. 14 shows the comparison between the mathematical solution and numerical results from OGS and RockFlow.
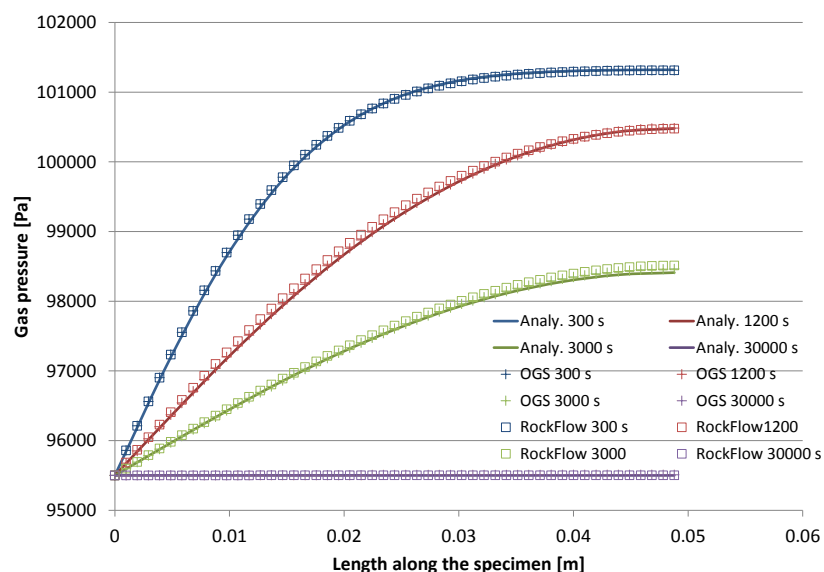

Fig. 14: Comparison between analytical solution and numerical results from OGS and RockFlow

4.2 Laboratory tests

Two laboratory gas injection tests have been introduced in Chapter 2. Both tests were simulated with the above mentioned numerical model. A triangle grid with an axial symmetric geometry was used to simulate the laboratory tests (Fig. 15 left) (EP1). A hydrostatic loading boundary condition was applied. All boundaries were assumed as water and gas impermeable except the injection and outflow boreholes. The measured gas injection pressure was applied in the injection borehole and the gas pressure in the outflow borehole kept constant with 0.1 MPa (Fig. 15 right). The initial conditions, material properties and parameters for the permeability modification approaches (Eq. (13)) are summarised in Table 2. The unsaturated flow parameters were set according to the study by NAGRA (2008). An elasto-plastic model with Drucker-Prager yield criterion was applied for the deformation behaviour. The parameters of mechanics behaviour were chosen form the report by Bock (2009). Considering the bedding plane the permeability was anisotropic, which was oriented horizontally for both tests. No data on water saturation during the tests was available and water was also not detected in the outflow borehole, thus, an initial saturation between 0.7 and 0.9 was assumed (Popp et al, 2007).
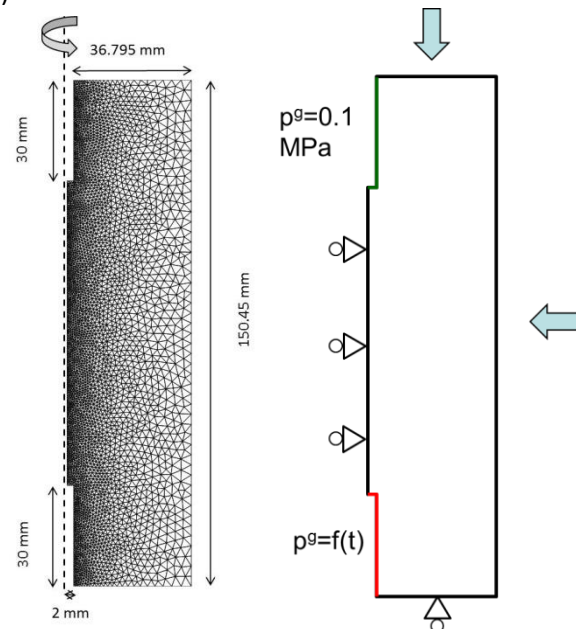

Fig. 15**:** Numerical model mesh (left) and schematic description of boundary conditions (right)

Table 2: Initial conditions and material properties

Parameter	Unit	Loading cycle test	Gas fracture cycle test.	Parameter	Unit	Loading cycle test	Gas fracture cycle test.
Initial p_g	Pa	1×10^5		Biot coefficient α	-	1.0	
Initial S_w	-	0.7	0.9	Porosity n	-	0.16	
Water viscosity	Pa·s	0.001		Gas viscosity η^w	Pa·s	1.6×10^{-5}	

η^w						
Gas entry pressure p_0	Pa	9×10^4	2.5×10^6	Young's module E	Pa	2.5×10^9
Water residual saturation $S_{w,r}$	-	0.5		Poison ratio v	-	0.27
Gas residual saturation $S_{g,r}$	-	0		Cohesion c	Pa	4.5×10^5
Factor of van Genuchten m	-	2		Friction angle ϑ	°	30
Permeability parallel $k_{//}$	m^2	2.1×10^{-16}	3.7×10^{-17}	Dilation angle φ	°	0
Permeability perpendicular $k_\perp$	m^2	2.1×10^{-17}	3.7×10^{-18}	Tensile strength σ^t	Pa	2.33×10^5
a_1	-	0.125		a_2	-	152
p_{thr}	MPa	3.2		b_1	-	4000
b_2	-	600		b_3	-	50

4.2.1 Loading cycle test

The numerical results of the gas outflow rate were compared with the measured data (Fig. 16). In the first phase of the experiment (from 0 to 3800 s) the calculated results of gas outflow rate with both permeability approaches were in good agreement with the measured data. Due to the relatively low gas entry pressure, at the beginning the gas could flow through the specimen, even if the injection pressure was low (0.2 MPa). The outflow rate increased proportionally to the injection pressure, and the permeability increased only slightly under conditions in which the gas pressure was lower than the confining pressure. When the confining pressure started to increase, the numerical results using the gas pressure dependent permeability approach could not be compared with the measured data because the permeability remained constant due to constant gas pressure. With the deformation dependent permeability approach the numerical results show a reasonable trend prediction. Due to the increase in confining pressure, a drop in the outflow rate was observed. The permeability was decreased due to the compression of the pore space. During the laboratory test between 3000 s and 4000 s, the unexpected outflow rate variation was potentially the result of discontinuous gas transport due to the local heterogeneous structure of the specimen (Popp et al., 2007).
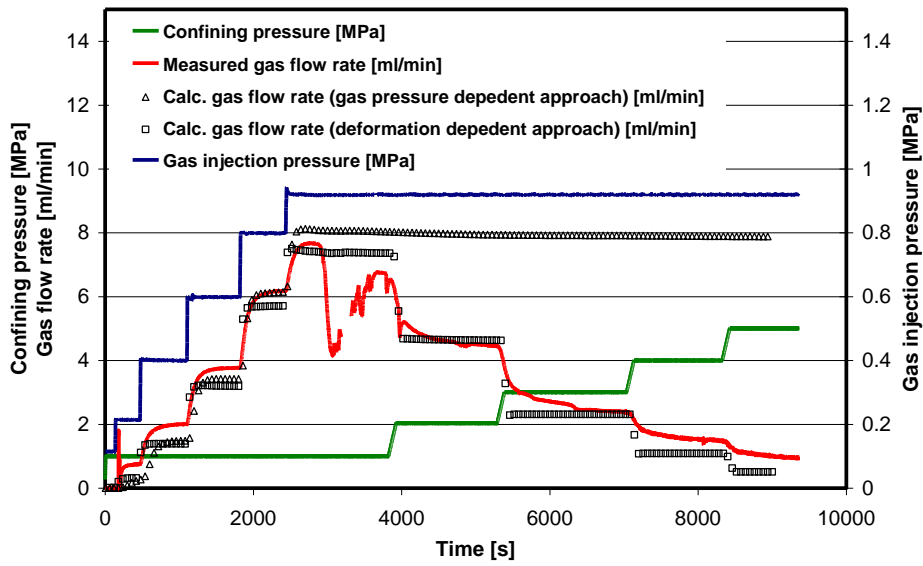
Fig. 16: Numerical results and laboratory measurement of loading cycle test

4.2.2 Gas fracture cycle experiment

The gas fracture cycle experiment had four phases considering the measured gas outflow rate, i.e. no outflow, slight increase, significant increase and final decrease of gas outflow rate (Fig. 17). Due to the low injection pressure at the beginning almost no gas outflow was measured in the extraction borehole. When gas injection pressure reached 2.5 MPa, the gas outflow was measured. The two-phase flow controlled gas transport took place. The outflow rate increased slightly, when gas injection pressure increased stepwise from 2.5 to 3.2 MPa. It should be noted that no significant increase of gas outflow rate was measured even if the injection pressure exceeded the confining pressure (3.0 MPa). When the injection gas pressure reached 3.5 MPa, the gas outflow rate increased significantly. It was evident that flow pathways with high permeability were generated in the specimen. The significantly increased permeability could be represented by both permeability approaches.
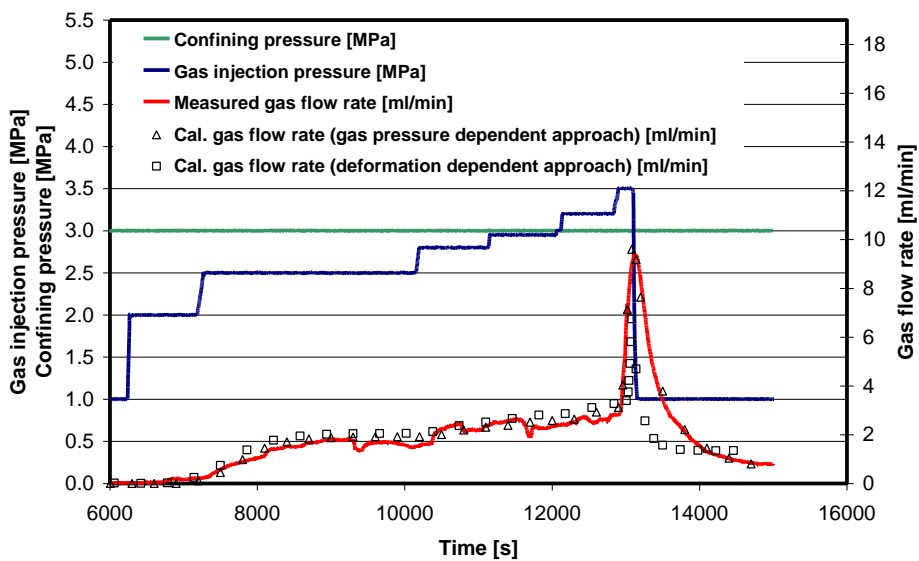

Fig. 17: Numerical results and laboratory measurement of fracture cycle test

4.3 In-situ borehole tests

A cubic model was established to simulate the test interval and near field of the test boreholes. Four boreholes (blue) and the packer (red) in BHG-B9 were involved in the numerical model (Fig. 18). The borehole axis was parallel to the global Y direction. The stress field was applied on the model boundaries. For the hydraulic process, boundary conditions had the same value as the initial conditions, and were applied on all model boundary surfaces besides the front surface, which was defined as an impermeable boundary. The gas pressures in the seismic boreholes were fixed as atmospheric pressure as well as the not sealed section in the injection borehole out of the packer.
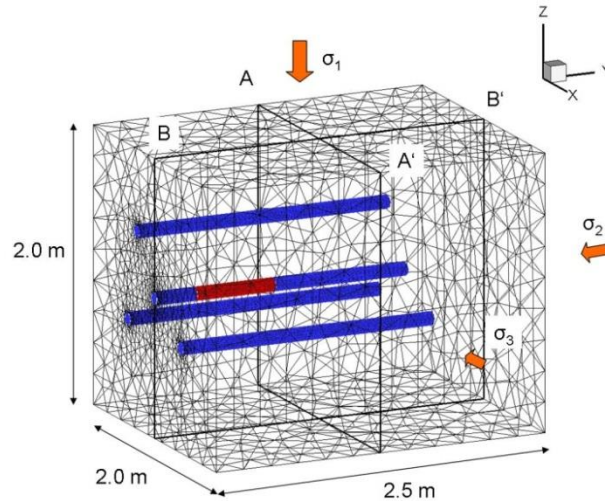

Fig. 18: Set up of the numerical model

For numerical interpretation we focus on the first series of the gas tests, which included 5 test phases with the injection gas pressure at 0.2, 0.6, 1.2, 1.8 and 2.2 MPa (EP2). The injected gas pressure in the test section was defined at the beginning of each test phase as an initial value in the model, and the gas pressure evolution afterwards was then simulated.

All parameters are listed in Table 3. Similar to the modelling of the laboratory experiments, transverse isotropic permeability was applied and the bedding plane was oriented perpendicular to the boreholes. The deformation behaviour was calculated by elasto-plastic model with Mohr-Coulomb criterion.

Table 3: Material properties and parameters for in-situ borehole tests NAGRA (2002, 2008)

Parameter	Unit	Value	Parameter	Unit	Value
Initial p_c	Pa	1.5×10^5	Biot coefficient α	-	1
Initial p_g	Pa	2×10^5	Poisson ratio v	-	0.27
Initial S_w	-	0.99	Friction angle ϕ	°	24.1
Gas entry pressure p_0	Pa	1×10^6	Dilation angle φ	°	0
Residual water saturation $S_{w,r}$	-	0.1	Cohesion c	Pa	1.9×10^6
Residual gas saturation $S_{g,r}$	-	0	Tensile strength σ^t	Pa	5×10^5

Water viscosity η^w	Pa·s	0.001	Gas viscosity η^g	Pa·s	1.6×10^{-5}
Factor of van Genuchten m	-	2	Permeability parallel $k_{//}$	m^2	1×10^{-20}
Porosity n	-	0.12	Permeability perpendicular $k_\perp$	m^2	1×10^{-21}
Young's module E	Pa	7×10^9			

Fig. 19 shows the comparison between the measured gas pressure and the numerical results using pressure dependent and deformation dependent permeability approaches. The calculated results have a similar trend of gas pressure development as the measured data. The gas pressure decreases faster under higher injection pressure.
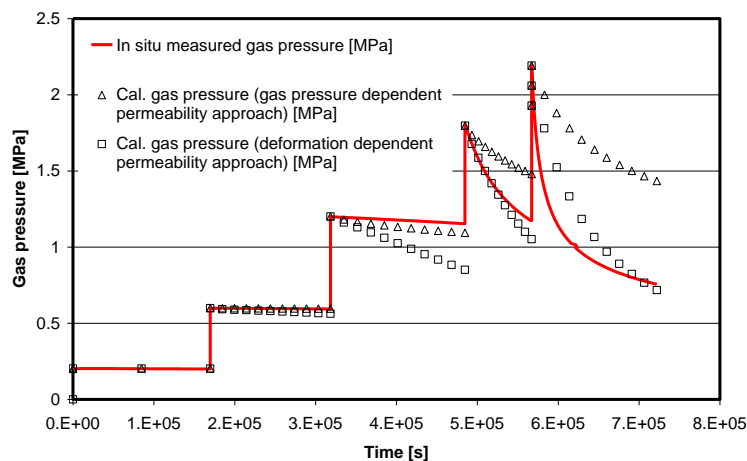

Fig. 19: Comparison between measured data and calculated gas pressure

Using the pressure dependent permeability approach, the gas transport process was controlled only by the hydraulic behaviour of the rock mass. The model calculation showed that the region affected by gas injection covered all seismic boreholes (BHG-B6, BHG-B7, and BHG-B8) (Fig. 20, left). The calculated results indicated that the seismic boreholes acted as sinks and both gas and water could flow out due to the constant atmospheric pressure in those boreholes. The increase of permeability was proportional to the gas pressure. Until the injection pressure reached 2.2 MPa, the maximum increase of permeability was about two orders of magnitude and within the bedding plane the dominate areas between the injection borehole and seismic boreholes had a permeability increase of more than 40 times the initial value (Fig. 20, right).
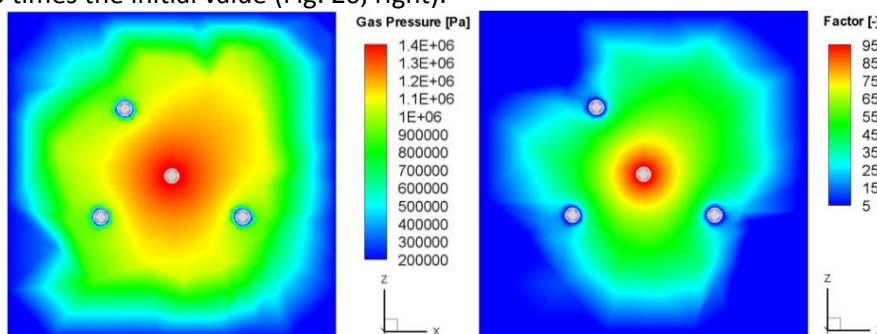

Fig. 20: Gas pressure distribution (left) and permeability modification factor (right) using pressure dependent approach at injection gas pressure 2.2 MPa

The deformation dependent permeability approach was based on coupled hydro-mechanical aspects. The permeability development was affected by the mechanical properties and anisotropic in-situ stress conditions. The plastic zone around the injection borehole was generated and developed during the gas injection tests. The distributions of gas pressure and equivalent plastic strain at the stage of 0.2, 0.6, 1.2, 1.8 and 2.2 MPa gas injection pressure were presented in Fig. 21. Due to high deviatoric stress, the development of the plastic zone was dominated by shear failure. The permeability increased significantly in the plastic zone, and was therefore calculated by about 1000 times higher (10^{-17} m²) than the initial intrinsic permeability (10^{-20} m²), which was also determined from the followed in-situ measurements. Consequently, most gas flowed in the higher permeability area, and the gas pressure distribution in the bedding plane was not more isotropic.
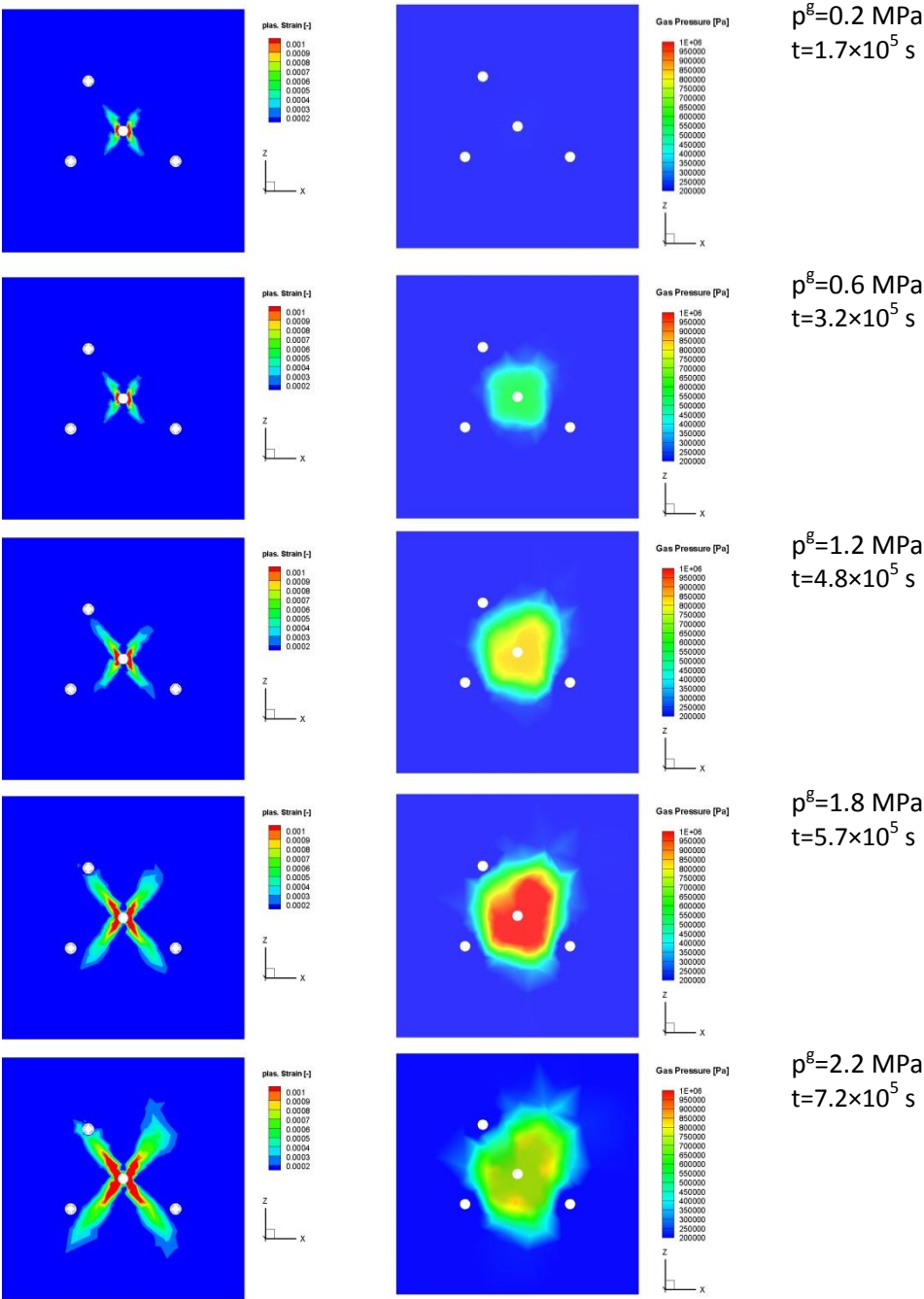

Fig. 21: Distribution of equivalent plastic strain and gas pressure at each gas injection step

The calculation results indicated a very possible flow path between BHG-B9 and BHG-B8. The gas injections section was connected with the seismic borehole through the generated flow pathway. Additionally there was also a plastic zone around the packer in the injection borehole, which indicated a connection between the packed-off interval and the borehole test section (Fig. 22). This phenomenon was well known as the flow paths around sealing (Lanyon et al., 2009).
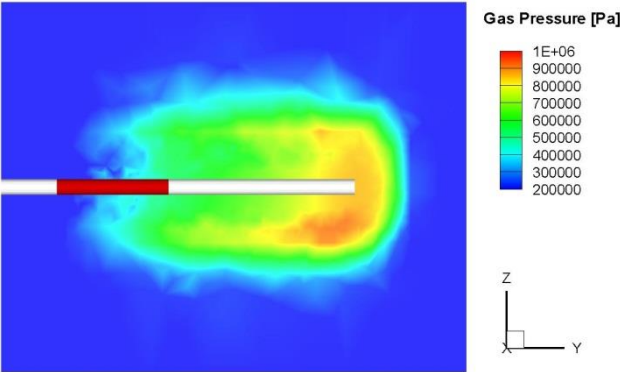

Fig. 22: Gas pressure distribution at the end of the injection stage with 2.2 MPa pressure

4.4 In-situ tunnel tests

A 3D coupled H^2M numerical model was built to simulate the HG-A injection tests (Fig. 23) (EP3). It involves 6 material groups, the rock (grey), the test section (blue), the packer (green), the liner section (red), the EDZ (yellow) and the flow resistance zone (black). The 0.3 m wide EDZ of high permeability around the micro-tunnel dominated the flow process. However, the EDZ around the tunnel was not uniform, due to the anisotropic stress field and the bedding structure of the rock. All important material parameters are summarised in Table 4.
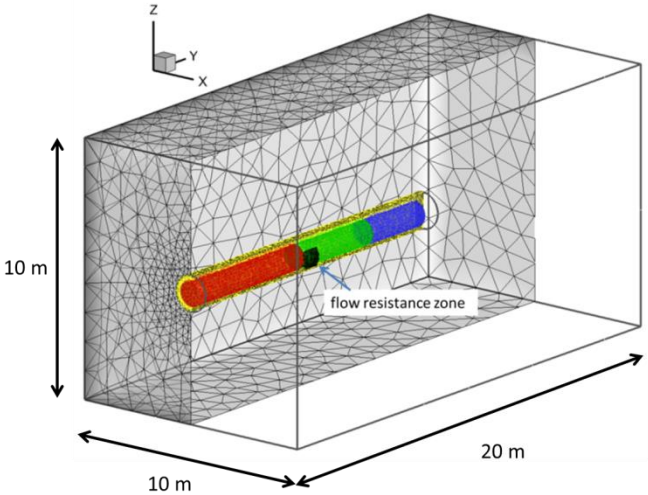

Fig. 23: Model set up for the in-situ tunnel tests

Table 4: Parameters for in-situ tunnel tests modelling

Parameter	Unit	Rock	EDZ	Test section
Porosity n	-	0.15	0.15	0.5
Permeability k^{int}	m^2	10^{-20}	10×10^{-18}	5×10^{-13}

Permeability $k^{int}\perp$		10^{-21}		
Residual water saturation $S_{w,r}$	-	0	0	0
Residual gas saturation $S_{g,r}$	-	0.05	0.05	0
Gas entry pressure p_0	MPa	2	0.2	0.013
Shape factor of van Genuchten eq. m	-	2	2	2
Young's moduli $E\parallel$	MPa	8000	8000	2000
Young's moduli $E\perp$	MPa	4000	4000	
Poisson ratio $\nu\parallel$	-	0.35	0.35	0.48
Poisson ratio $\nu\perp$	-	0.25	0.25	
Biot's coefficient α	-	1	1	1
Friction angle of MC criterion ϕ	°	20	20	-
Uniaxial strength f_c	MPa	Fig. 12	Fig. 12	-
Water viscosity μ^w	Pa s	0.001		
Gas viscosity μ^g	Pa s	1.7×10^{-5}		

The excavation of HG-A tunnel was simulated with an anisotropic elastic perfect plastic model (Chapter 3). The generation of highly damaged zone were controlled by two major mechanisms (Lanyon 2011): 1) Stress state exceeded the shear failure strength due to the stress redistribution after excavation. 2) Due to the anisotropic mechanical behaviour of Opalinus Clay, cracks were generated between the bedding planes in form of volume extension. The numerical results predicted the generation of breakouts and were well agreed with the in-situ laser scan results (Fig. 24).
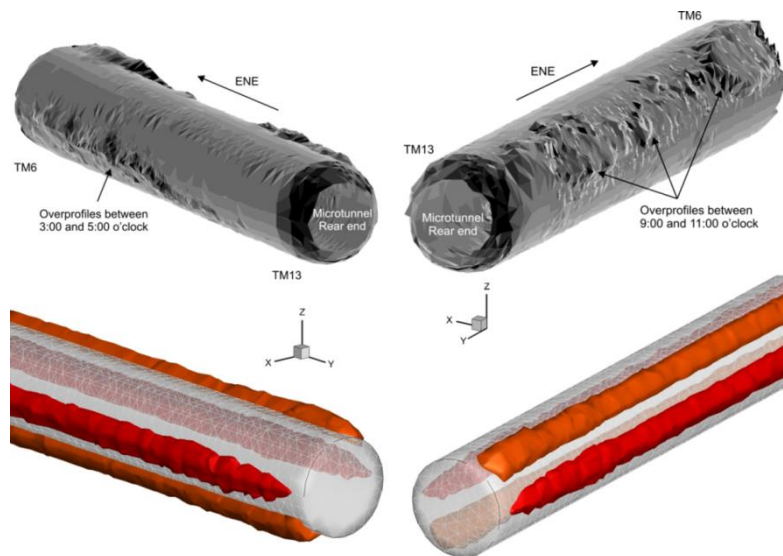

Fig. 24: Comparison between the numerical results of shear failure and extension zone with the in-situ 3D laser scan results (Nussbaum et al. 2005)

The numerical results of flow vector (Fig. 25) shows that the flow paths in the highly damaged zone at 9 o'clock position dominate the hydraulic process. Only the deformation dependent permeability approach is used to simulate the permeability increase in the highly damaged zone.
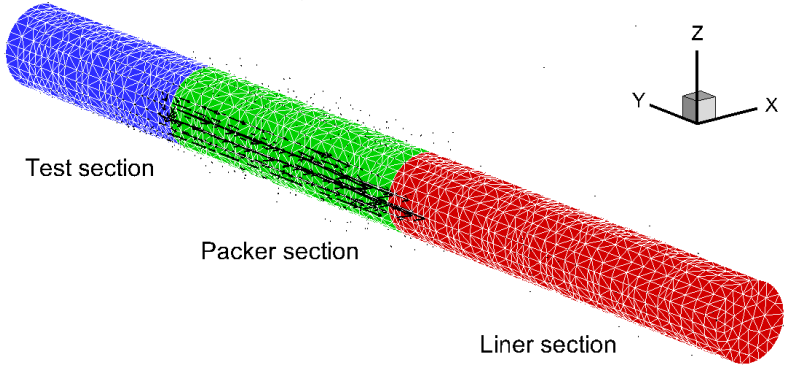

Fig. 25: Numerical results of flow vector

The calculated distribution of water saturation during the first gas test is presented in Fig. 26. The test section was refilled with gravel, which was high permeable and had low gas entry pressure. Thus, it is easier for the gas phase to displace the water in the test section than the water in the rock. The rock around the test section was almost fully saturated. According to the applied relative permeability model the permeability of the gas phase is extremely low. Therefore, the injected gas accumulated at the ceiling of the tunnel. The numerical results indicate an excellent gas sealing function of the system.
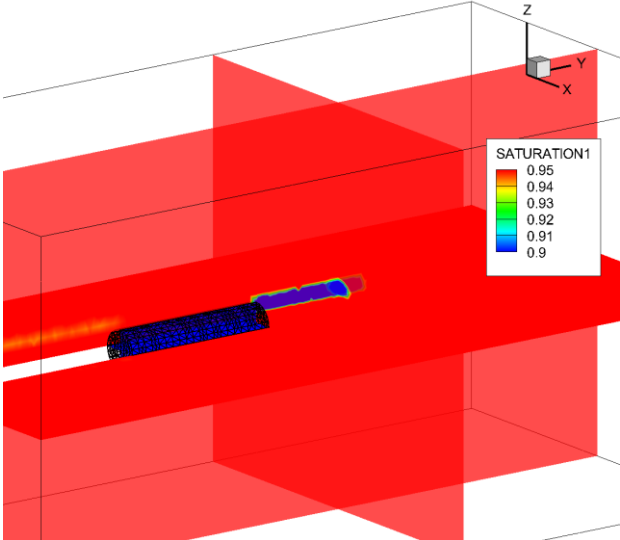

Fig. 26: Numerical results of saturation distribution by first gas test

Fig. 27 shows the calculated pressure distribution at the 3, 6, 9 and 12 o'clock positions compared with the measured data. The numerical results predict well the pressure distribution in the packer section as compared with the in-situ measurement. The pressure gradient between the three measurement sensors in the 3 o'clock position is small, because of the local high permeability. The existence of a flow resistance zone between PES1_3H and the liner section is indicated. The pressure at 6 o'clock position was higher than at the 9 and 12 o'clock positions, due to the higher pressure at the 3 o'clock position and the highly permeable area between the 3 and 6 o'clock positions, where breakouts existed. More details of the hydraulic behaviour of the EDZ around the tunnel can be found in EP3.
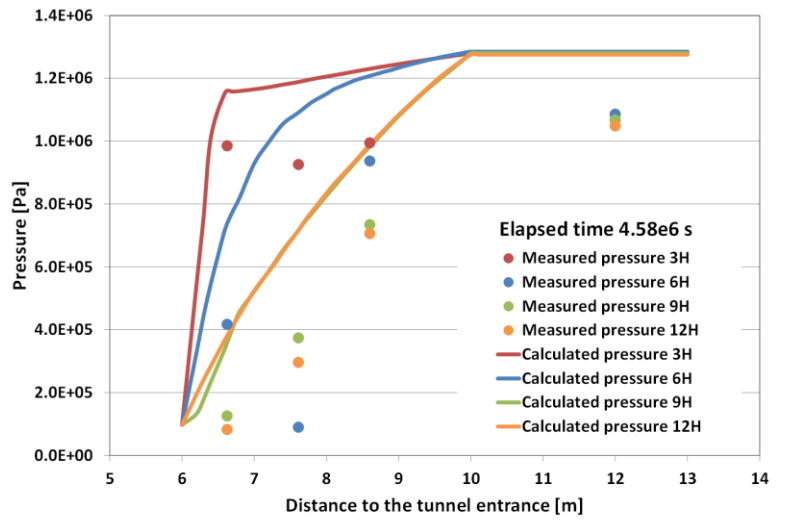
Fig. 27: Comparison between the calculated pressure along the tunnel at 3, 6, 9, and 12 o'clock positions with measure data

Fig. 28 shows the measrued and calculated pressure in the test section durign the first two gas injection tests. With the developed numerical model the calculated results can well represent the pressure evolution trend. Pressure breakdown was observed when the pressure reached 1.35 MPa. It was possibly caused by the generation of new flow paths or extension of the existing flow paths. After that, The measured pressure remained almost constant at 1 MPa.

Fig. 28: Measured and calculated pressure in the test section during the first two gas injection tests

5. Conclusions and outlooks

In this work a coupled multiphase-flow and mechanical (H^2M) model was developed. The model takes into account both hydraulic and mechanical anisotropic behaviour of the Opalinus Clay and the permeability variation due to d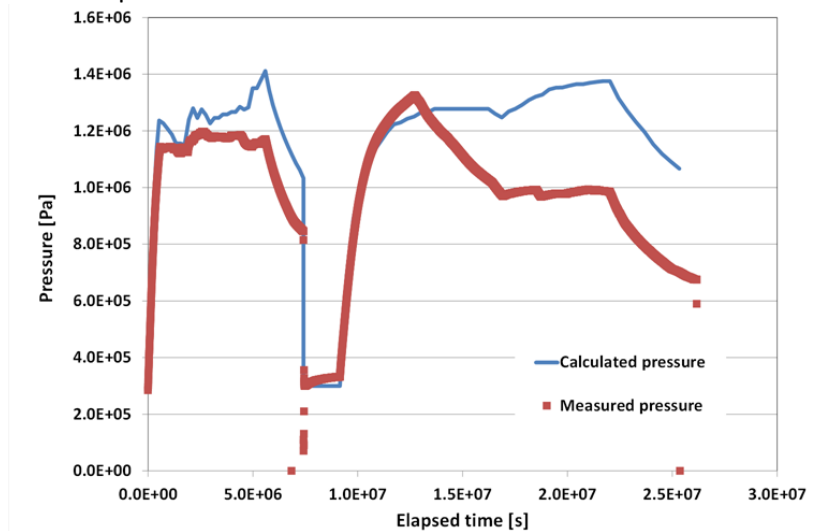eformation. The aim of the developed model was to investigate the gas migration process in saturated Opalinus Clay. Two flow regimes were successfully modelled: the tow-phase flow controlled regime with slight permeability change when gas pressure reaches the entry pressure, and the flow paths dilatancy controlled regime with significant permeability increase when the gas pressure exceeded the critical level. The gas migration mechanisms were studied with simulation of the gas injection tests at different scales. The measured data were compared with the numerical results, and some important observations during the tests were interpreted and analysed.

The developed numerical model is appropriate for simulation the gas injection test at different scales, i.e. laboratory test, in-situ borehole test and in-situ tunnel test. Under the laboratory conditions the test measurement can be extremely well represented by the numerical results. At the in-situ scale the test conditions will be more complicated. With considering the deformation dependent permeability the in-situ gas injection tests can quantitatively analysed using the numerical model.

The anisotropic permeability of the Opalinus Clay controls the gas migration at low gas pressure level. The gas transport velocity in the bedding plane was higher than in the perpendicular direction to the bedding. The permeability change was limited when the gas pressure under the threshold value. Due to the in-situ drilling operation, damage zone were generated around the borehole or tunnel. The permeability in the damage zone was significantly increased, and these high permeable areas dominated the gas transport. With the applied model the in-situ observed generation of the damaged zone and the measured hydraulic behaviour could be represented. Thus, the deformation dependent permeability approach is more appropriate for the gas migration investigation under the complicate in-situ conditions.

In the future work the numerical model can be improved with considering several additional impact factors. For example, the dissolved gas in pore water should be involved to complete the gas migration mechanisms in porous media under the low gas pressure condition. The thermal process will be considered to simulate a radioactive waste repository with heat emission. Besides permeability, other material properties can also be impacted due to the damage, e.g. the gas entry pressure, porosity and stiffness.

REFERENCES

Alonso EE, Olivella S, Arnedo D (2006): Mechanisms of gas transport in clay barriers. Journal of Iberian Geology 32 (2): 175-196

Bock H (2009): Updated Review of the Rock Mechanics Properties of the Opalinus Clay of the Mont Terri URL based on Laboratory and Field Testing. Mont Terri Technical Report 2008-04, Q+S Consult, Germany

Boisson JY, Bertrand L, Heitz JF, Golvan Y (2001): In situ and laboratory investigations of fluid flow through an argillaceous formation at different scales of space and time, Tournemire tunnel, southern France. Hydrogeology Journal, 9(1), 108–123. doi:10.1007/s100400000119

Clausen J (2007): Efficient non-linear finite element implementation of elasto-plasticity for geotechnical problems. Ph.D. thesis, Esbjerg institute of technology, Aalborg University

Crisfield MA (1997): Non-Linear Finite Element Analysis of Solids and Structures, Volume 2: Advanced Topics. John Wiley & Sons. ISBN 978-0471956495

Croisé J, Mayer G, Marschall P, Matray JM, Tanaka T, Vogel P (2006): Gas Threshold Pressure Test Performed at the Mont Terri Rock Laboratory (Switzerland): Experimental Data and Data Analysis, Oil & Gas Science and Technology - Rev. IFP, Vol. 61 (2006), No. 5, pp. 631-645. doi: 10.2516/ogst:2006003

Davy AC, Skoczylas F, Barnichon JD, Lebon P (2007): Permeability of macro-cracked argillite under confinement: Gas and water testing. Physics and Chemistry of the Earth, Parts A/B/C, 32(8-14), 667–680. doi:10.1016/j.pce.2006.02.055

Gräsle W, Plischke I (2010): Laboratory testing (LT) experiment: mechanical behavior of Opalinus Clay. Final report from Phases 6–14. Mont Terri Project Technical Report 2009-07

Guimaraes L, Gens A, Olivella S (2007): Coupled thermo-hydro-mechanical and chemical analysis of expansive clay subjected to heating and hydration. TRANSPORT IN POROUS MEDIA, 66(3): 341-372.

Helmig R, (1997): Multiphase flow and transport processes in the subsurface: a contribution to the modelling of hydrosystems. Springer, ISBN 3-540-62703-0.

Hou Z, Lux KH (2004): A new coupling concept for the hydro-mechanical interaction of clay stone and rock salt in underground waste repositories. International Journal of Rock Mechanics and Mining Sciences, 41, 708-713.

Hou Z, Gou Y, Taron J, Gorke UJ, Kolditz O (2012): Thermo-hydro-mechanical modeling of carbon dioxide injection for enhanced gas-recovery (CO2-EGR): a benchmarking study for code comparison. Environmental Earth Sciences, 67(2), 549–561. doi:10.1007/s12665-012-1703-2

Hudson J, Stephansson O, Andersson J, Tsang CF, Jing L (2001): Coupled T–H–M issues relating to radioactive waste repository design and performance. International Journal of Rock Mechanics and Mining Sciences, 38(1): 143–161.

Itasca Consulting Group, Inc. (2009): FLAC3D (Fast Lagrangian Analysis of Continua in 3 Dimensions), Version 4.0, Minneapolis.

Jing L, Tsang CF, Stephansson O (1995): DECOVALEX—an international cooperative research project on mathematical models of coupled THM processes for safety analysis of radioactive waste repositories. Int J Rock Mech Min Sci 32:389–398.

Kolditz O, Zielke W (1996): RockFlow Benchmarks: Examples in subsurface hydrology.

Kolditz O, de Jonge J, Beinhorn M, Xie M, Kalbacher T, Wang W, Kohlmeier M (2003): ROCKFLOW-Theory and user's manual, release 3.9. Groundwater Group, Center for Applied Geosciences, University of Tübingen, and Institute of Fluid Mechanics, University of Hannover.

Kolditz O, Görke UJ, Shao H, Wang W (eds) (2012a): Thermo-Hydro-Mechanical-Chemical Processes in Fractured Porous Media. Springer, Heidelberg.

Kolditz O, Bauer S, Bilke L, Böttcher N, Delfs JO, Fischer T, Görke UJ, Kalbacher T, Kosakowski G, McDermott CI, Park CH, Radu F, Rink K, Shao H, Shao HB, Sun F, Sun YY, Singh AK, Taron J, Walther M, Wang W, Watanabe N, Wu N, Xie M, Xu W, Zehner B (2012b): OpenGeoSys: an open-source initiative for numerical simulation of thermo-hydro-mechanical/chemical(THM/C) processes in porous media. Environmental Earth Sciences doi: 10.1007/s12665-012-1546-x.

Lanyon GW (2011): Excavation Damaged Zones Assessment. NWMO DGR-TR-2011-21.

Lanyon GW, Marschall P, Trick T, de La Vaissière R, Shao H, Leung H (2009): Hydromechanical Evolution and Self-Sealing of Damage Zones around a Microtunnel in a Claystone Formation of the Swiss Jura Mountains. The 43rd US Rock Mechanics Symposium and 4th U.S.-Canada Rock mechanics Symposium, Asheville, NC, USA.

Lewis RW, Schrefler BA (1998): The Finite Element Method in the Static and Dynamic Deformation and Consolidation of Porous Media, second ed. Wiley, New York, USA, 508 pp.

Liu QS, Zhang CY, Liu XY (2006): Numerical modelling and simulation of coupled THM processes in Task_D of DECOVALEX_IV. Chinese Journal of Rock Mechanics and Engineering, 25 (4), pp. 709–720

Lydzba D, Pietruszczak S, Shao JF (2003): On anisotropy of stratified rocks: homogenization and fabric tensor approach. Computers and Geotechnics 30: 289-302. doi: 10.1016/S0266-352X(03)00004-1.

Marschall P, Croisé J, Schlickenrieder L, Boisson JY, Vogel P, Yamamoto S (2003): Synthesis of hydrogeological investigations at the Mont Terri site (Phases 1 - 5). Mont Terri Technical Report TR 2001-02, Geotechn. Inst. Ltd., Bern, Switzerland.

Marschall P, Horseman S, Gimmi T (2005): Characterisation of Gas Transport Properties of the Opalinus Clay, a Potential Host Rock Formation for Radioactive Waste Disposal. Oil & Gas Science and Technology - Rev. IFP, Vol. 60, No. 1, pp. 121-139. doi: 10.2516/ogst:2005008

Marschall P, Distinguin M, Shao H, Bossart P, Enachescu C, Trick T (2006): Creation and Evolution of Damage Zones Around a Microtunnel in a Claystone Formation of the Swiss Jura Mountains. International Symposium and Exhibition on Formation Damage Control, Louisiana U.S.A., doi: 10.2118/98537-MS

NAGRA (2004): Effects of Post-disposal Gas Generation in a Repository for Spent Fuel, High-level Waste and Long-lived Intermediate Level Waste Sited in Opalinus Clay. Nagra Tech. Rep. 04-06.

NAGRA (2008): Effects of Post-disposal Gas Generation in a Repository for Low- and intermediate-level Waste Sited in the Opalinus Clay of Northern Switzerland. Nagra Tech. Rep. 08-07.

Naumann M, Hunsche U, Schulze O (2007): Experimental investigations on anisotropy in dilatancy, failure and creep of Opalinus Clay. Physics and Chemistry of the Earth 32: 889-895. doi: 10.1016/j.pce.2005.04.006

Nussbaum C, Badertscher N, Métille J, Meier O, Bossart P (2005): HG-A experiment: Detailed structural mapping of the microtunnel walls. Mont Terri Project Technical Note 2005-49.

Noorishad J, Tsang CF (1996): ROCMAS simulator; A thermo-hydro-mechanical computer code. Developments in Geotechnical Engineering, Vol. 79, Pages 551–558. doi: 10.1016/S0165-1250(96)80045-9

Olivella S, Alonso EE (2008): Gas flow through clay barriers. Géotechnique 58, No. 3, 157-176.

Ohnishi Y, Shibata H, Kobayashi A (1987): Development of finite element code for the analysis of coupled thermo-hydro-mechanical behaviors of a saturated-unsaturated medium. C.F. Tsang (Ed.), Coupled Processes Associated with Nuclear Waste Repositories, Academic Press, Orlando, pp. 551–557

Pietruszczak S, Mroz Z (2000): Formulation of anisotropic failure criteria incorporating a microstructure tensor. Computers and Geotechnics 26: 105-112. doi: 10.1016/S0266-352X(99)00034-8

Pietruszczak S, Mroz Z (2001): On failure criteria for anisotropic cohesive-frictional materials. International Journal for Numerical and Analytical Methods in Geomechanics 25,509-524. doi: 10.1002/nag.141

Pietruszczak S, Lydzba D, Shao JF (2002): Modelling of inherent anisotropy in sedimentary rocks. International Journal of Solids and Structures 39: 637-648. doi: 10.1016/S0020-7683(01)00110-X

Popp T, Wiedemann M, Böhnel H, Minkley W (2007): "Untersuchungen zur Barriereintegrität im Hinblick auf das Ein-Endlager-Konzept". Institut für Gebirgsmechanik GmbH, Leipzig, Germany.

Rutqvist J, Tsang CF (2003): TOUGH-FLAC: a numerical simulator for analysis of coupled thermal-hydrologic-mechanical processes in fractured and porous geological media under multi-phase flow conditions. In Proceedings of the TOUGH Symposium (pp. 12-14).

Saaltink MW, Ayora C, Olivella S (2005): User's guide for RetrasoCodeBright (RCB). Department of Geotechnical Engineering and Geo-Sciences, Technical University of Catalonia (UPC), Institute of Earth Sciences Jaume Almera, Spanish Research Council (CSIC), Barcelona, Spain.

Sanavia L, Pesavento F, Schrefler B.A. (2006): Finite element analysis of non-isothermal multiphase geomaterials with application to strain localization simulation. Comput Mech Vol. 37: 331-348. doi: 10.1007/s00466-005-0673-6

Senger R, Enachescu C, Doe T, Distinguin M, Delay J, Frieg B (2006): Design and analysis of a gas threshold pressure test in a low-permeability clay formation at ANDRA's underground research laboratory, Bure (France). TOUGH Symposium, Lawrence Berkeley National Laboratory, Berkeley, California.

Senger R, Lanyon B, Marschall P, Vomvoris S, Fujiwara A (2008): Numerical Modelling of the Gas Migration Test at the Grimsel Test Site (Switzerland). TOUGH Symposium 2006, Berkeley, California , ETATS-UNIS (05/2006), vol. 164, 2, pp. 155-168

Shao H, Schuster K (2009): Permeability Measurements of Opalinus Clay (Mont Terri) HG-B: Combined Permeability Tests and Borehole Seismic Measurements. Internal Report. B3.1-10856/2009, BGR, Hanover, Germany.

Schlömer S, & Krooss BM (1997): Experimental characterisation of the hydrocarbon sealing efficiency of cap rocks, Mar. Pet. Geol. 14(5), 565–580.

Stephansson O, Hudson JA, Jing L (eds) (2004): Coupled thermo-hydro-mechanical-chemical processes in geo-systems: fundamentals, modelling, experiments and applications. Elsevier, Oxford, 831

Thury M, Bossart P (1999): The Mont Terri rock laboratory, a new international research project in a Mesozoic shale formation, in Switzerland. Engineering Geology, 55: 347-35

Tsang CF, Stephansson O, Jing L, Kautsky F (2009): DECOVALEX Project: from 1992 to 2007. Environmental Geology, 57:1221–1237.

Tsang CF, Barnichon JD, Birkholzer J, Li XL, Liu HH, Sillen X (2012): Coupled thermo-hydro-mechanical processes in the near field of a high-level radioactive waste repository in clay formations. International Journal of Rock Mechanics and Mining Sciences, 49, 31–44. doi:10.1016/j.ijrmms.2011.09.015

Van Genuchten MTh (1980): A closed-form equation for predicting the hydraulic conductivity of unsaturated soils. Soil Science Society of America Journal, Vol. 44 No. 5, p. 892-898. doi: 10.2136/sssaj1980.03615995004400050002x

Vomvoris S, Lanyon B, Marschall P, Ando K, Adachi T, Fujiwara A, Yamamoto S (2002): Sand/Bentonite Barriers and Gas Migration: The GMT Large-Scale In-Situ Test in the Grimsel Test Site. MRS Proceedings, 757, II3.27 doi:10.1557/PROC-757-II3.27.

Wang W, Kosakowski G, Kolditz O (2009): A parallel finite element scheme for thermo-hydro-mechanical (THM) coupled problem in porous media. Computers and Geosciences 35(8): 1631-1641, doi: 10.1016/j.cageo.2008.07.007

Wang W, Rutqvist J, Gorke UJ, Birkholzer JT, Kolditz O (2011): Non-isothermal flow in low permeable porous media: A comparison of unsaturated and two-phase flow approaches. Environmental Earth Sciences 62 (6): 1197 – 1207, doi: 10.1007/s12665-010-0608-1.

Watanabe N, Wang W, Mcdermott CI, Kolditz O (2009): Thermo-Hydro-Mechanical Modelling and Applications for Enhanced Geothermal Reservoirs. GRC Transactions, Vol.33.

Yang D, Billiotte J, Su K (2010): Characterization of the hydromechanical behavior of argillaceous rocks with effective gas permeability under deviatoric stress. Engineering Geology, 114(3-4), 116–122. doi:10.1016/j.enggeo.2010.04.002

Zhang CL, Rothfuchs T (2004): Experimental study of the hydro/mechanical behaviour of the Callovo/Oxfordian argillite. Applied Clay Science 26, 325-336.

Zhou L, Hou MZ (2013): International Journal of Rock Mechanics & Mining Sciences A new numerical 3D-model for simulation of hydraulic fracturing in consideration of hydro-mechanical coupling effects. International Journal of Rock Mechanics and Mining Sciences, 60, 370–380. doi:10.1016/j.ijrmms.2013.01.006

List of Publication

First author publications peer-reviewed international journals

[EP1] **Xu WJ**, Shao H, Hesser J, Wang W, Kolditz O, Popp T (2011) Simulation of dilatancy-controlled gas migration process in saturated argillaceous rock. Computational Geomechanics, COMGEO II, Proceedings of the 2nd International Symposium on Computational Geomechanics, pp. 693-703, ISBN: 978-960987501-1. (listed in SCOPUS)

[EP2] **Xu WJ**, Shao H, Hesser J, Wang W, Schuster K, Kolditz O (2013) Coupled multiphase flow and elsto-plastic modelling of in-situ gas injection experiments in saturated clay stone (Mont Terri Rock Laboratory). Engineering Geology, 157: 55-68, doi: 10.1016/j.enggeo.2013.02.005. (ISI listed)

[EP3] **Xu WJ**, Shao H, Marschall P, Hesser J, Kolditz O (2013) Analysis of flow path around the sealing section HG-A experiment in the Mont Terri Rock Laboratory. Environ. Earth Sci., doi: 10.1007/s12665-013-2403-2. (ISI listed)

Additional publications

[EP4] Kolditz O, Bauer S, Bilke L, Böttcher N, Delfs JO, Fischer T, Görke UJ, Kalbacher T, Kosakowski G, McDermott CI, Park CH, Radu F, Rink K, Shao H, Shao HB, Sun F, Sun YY, Singh AK, Taron J, Walther M, Wang W, Watanabe N, Wu N, Xie M, **Xu W**, Zehner B (2012b) OpenGeoSys: an open-source initiative for numerical simulation of thermo-hydro-mechanical/chemical(THM/C) processes in porous media. Environ. Earth Sci., 67(2): 589-599, doi: 10.1007/s12665-012-1546-x

Book chapter

[EP5] **Xu WJ**, Wang W, Watanabe W, Hesser J, Krug S (2012) Thermomechanics. In Kolditz O, Görke UJ, Shao H, Wang W (editors), Thermo-Hydro-Mechanical-Chemical Processes in Fractured Porous Media. Springer, Heidelberg.

Theses

1. Multiphase-flow controlled and flow pathway dilatancy controlled gas migration processes are most important two mechanisms during the gas migration in argillaceous rock. The gas migration processes at different scales are studied and can be successfully simulated with the applied numerical model.

2. A coupled multiphase-flow and mechanical model is developed and implemented into the FEM numerical codes OpenGeoSys (OGS). The porous medium is assumed to be continue and homogenous. The effective stress concept for unsaturated medium is used to consider the pressure effect on the deformation process.

3. The strongly anisotropic properties of hydraulic and mechanical behaviour of Opalinus Clay are involved in the model. A two order tensor is applied to consider the anisotropic permeability in 3-dimension. The anisotropic mechanical behaviour is described by generalized Hooke's law.

4. Two permeability modification approaches, gas pressure dependent and deformation dependent, are developed and applied to simulate the permeability change during the injection tests. Both approaches can well represent the laboratory tests with constant confining pressure. The deformation dependent approach is more appropriate for the laboratory tests with increased confining pressure and in-situ tests with complicate conditions.

5. The anisotropic elastic perfect plasticity is calculated with microstructure tensor method. The generation of plastic zone is modelled and the numerical results can well represent the test observations. According to the applied approach the permeability in these areas can significantly increase.

6. The developed numerical mode is validated. A transient gas out flow test is simulated and the results are compared with analytical solution and numerical results of RockFlow a former version of OGS-5.

7. The laboratory, in-situ borehole and in-situ tunnel gas injection tests are simulated and analysed. The measured pressure data can be well represented with the numerical model. According to the applied permeability modification approaches, the increased permeability can be 1000 times higher than its initial state in the highly permeable areas.

8. By the laboratory gas injection tests, the gas can flow through the specimens when the injection pressure is higher than the entry pressure, which is also varied by different specimens. During the compression operation the permeability is reduced. The gas out flow rate is increased significantly due to the flow pathway dilatancy, when the injection pressure is about 0.5 MPa higher than the confining pressure.

9. The numerical model is applied to analyse the in-situ borehole tests. The development of the flow pathway with increased injection pressure is simulated. The possible connection between the injection borehole and the observation borehole is indicated by the numerical results, which is also supported by the in-situ measurement.

10. The gas injection tests in HG-A tunnel is simulated and the flow paths around the tunnel is analysed. The measured pressured distribution around the tunnel and the pressure variation in the test section is quantitatively represented with the applied deformation dependent permeability approach. The highly permeable flow paths at 3 and 9 o'clock positions are indicated.

Thesen

1. Mehrphasenströmung kontrollierte und Fließwegdilatanz kontrollierte Gasmigrationsprozessen sind die zwei wichtigsten Mechanismen bei dem Gastranport in Tonstein. Die Gasmigrationsprozesse bei unterschiedlichen Maßstäben werden untersucht und können erfolgreich mit dem angewandten numerischen Modell simuliert werden.

2. Ein numerisches Modell für die Kopplung zwischen Mehrphasenströmung und Mechanik wird entwickelt und im FEM-Programm OpenGeoSys implementiert. Das Konzept der effektiven Spannung für teilgesättigtes Medium wird benutzt, um der Kopplungseffekt der Mehrphasenströmung auf den mechanischen Prozess zu berücksichtigen.

3. Die stark anisotropen Eigenschaften des hydraulischen und mechanischen Verhaltens von Opalinuston werden im Modell berücksichtigt. Die anisotropen Permeabilität wird von einem Tensor definiert. Das anisotrope mechanische Verhalten wird mit dem verallgemeinerten hookeschen Gesetz beschrieben.

4. Zwei Formulierungen für die Permeabilitätsmodifikation (Gasdruckabhängig und verformungsabhängig) werden entwickelt, um die Permeabilitätsänderung bei den Gasinjektionsversuchen zu simulieren. Beide Formulierungen können die Laborversuche mit konstantem Manteldruck quantitative repräsentieren. Die verformungsabhängige Formulierung ist mehr geeignet für die Versuchen mit steigenden Manteldruck und die In-situ Versuchen mit komplizierten Bedingungen.

5. Die anisotrope elasto-perfekt-plastizität wird mit „microstructure tensor" Verfahren berechnet. Die Generation der plastischen Zone wird simuliert. Die Versuchsbeobachtungen können von den numerischen Ergebnissen repräsentiert werden.

6. Das entwickelte Modell wird mit einem transienten Gasausströmungsversuch validiert. Die berechneten Ergebnisse werden mit der analytischen Lösung und die Ergebnisse von anderen Programm (RockFlow) vergleicht.

7. Die Labor-, In-situ-Bohrloch und In-situ-Tunnelversuchen werden simuliert und untersucht. Nach den angewandten Formulierungen der Permeabilitätsänderung kann die erhöhte Permeabilität im stark durchlässigen Bereich 100 bis 1000 Mal höher als den ungestörten Zustand.

8. Bei den Laborgasinjektionsversuchen kann Gas durch die Probekörper fließen, wenn der Injektionsdruck höher als den Eindringendruck ist. Während der Kompaktion wird die Permeabilität reduziert. Wegen der Fließwegdilatanz findet die erhebliche Erhörung der Gasausströmungsrate statt, wenn der Injektionsdruck 0.5 MPa höher als den Manteldruck.

9. Die Entwicklung der Fließwege mit dem erhöhten Druck bei den In-situ-Bohrlochversuchen wird simuliert. Die möglichen Verbindungen zwischen dem Injektionsbohrloch und dem Beobachtungbohrloch werden von der numerischen Modellierung hingewiesen.

10. Die Generation der stark geschädigten Zone in HG-A Tunnel wird von der Spannungsumlagerung und von dem anisotropen Verformungsverhalten des Opalinustons kontrolliert. Die stark durchlässigen Bereiche an 3 und 9 Uhr Position werden hingewiesen. Sie dominieren die Strömung durch die EDZ um den Packerbereich.